UNIVERSIDAD DE INGENIERÍA Y TECNOLOGÍA

CARRERA DE INGENIERÍA MECÁNICA

CHARACTERIZATION OF A SOFT PNEUMATIC ACTUATOR USING FE MODELLING

THESIS

Para optar el título profesional de Ingeniero Mecánico

AUTHOR

Sharonluz Steffi Torres Atencia (ORCID: 0000-0003-4275-8605)

ADVISOR

García – Bravo, José (ORCID: 0000-0002-3017-3354)

Newell, Brittany (ORCID: 0000-0001-5737-2065)

Noel, Julien (ORCID: 0000-0001-9284-9025)

Lima – Perú

2021

Dedication:

To my mother and father, for supporting my dreams and being by my side always. For always giving me strength when I felt that I could not keep going. For the effort to give me the best education. To my brother, for his unconditional love and guidance. To my friends that walked in this adventure with me and made the journey full of memories and enjoyable moments.

Acknowledgments:

I would like to thank UTEC and my parents for giving me the opportunity to do a double degree with Purdue University. Also, I would like to thank my advisors, Jose Garcia-Bravo and Brittany Newell, for the guidance and support in the project.

TABLE OF CONTENTS

TABLE INDEX

Pág.

FIGURE INDEX

Pág.

ANNEX INDEX

Pág.

OBJECTIVE

Characterize a 3D printed 5 chamber bellow using Dragon Skin Silicone by doing a FEA simulation to determine the maximum pressure and deformation

METHODOLOGY

Some common methods currently used in the process of printing soft actuators are spray forming, spray molding, selective laser melting, fused deposit modeling and stereolithography.

Spray forming consists in spraying liquid molding material to form layers until the desire geometry is achieved. Spray molding is similar to spray forming with the difference that it uses an adhesive that is sprayed on a powder layer. On the other hand, selective laser melting builds up the geometry layer by layer using a metal powder that is laser later. Fused deposit modeling is the most typical 3D printing method in which layers of the material are extruded through the nozzle of the printer, and the one that is going to be used for testing. Finally, stereolithography consists in forming the polymer that is cured using UV light

ABSTRACT

CHARACTERIZATION OF A SOFT PNEUMATIC ACTUATOR USING FE MODELLING

Actuators are devices that provides controlled changes regarding their displacement and position. They can be triggered by different inputs, one of them being fluids. Pneumatic actuators are commonly used in different areas. Rigid pneumatic actuators present multiple disadvantages, in size, weight, etc. limiting the application in other areas like soft robotic and biomechanics.

On the other hand, soft actuators possess big advantages in comparison with the rigid ones. The materials used give them an advantage in geometry, cost, etc. Yet, the development of this new technology is not fully understood due to the material properties in the manufacturing process. 3D printing is seen as one of the most feasible manufacturing processes for this new technology. However, the information regarding the topic is limited.

This study will focus into the characterization of 3D printed soft pneumatic actuator using as material silicone, especially in how the properties change when 3D printed with different printing orientations. Simulations were run using ANSYS and the results showed that the bellow printed at 90° has a higher resistance in the pressure applied and the 45° has a bigger deformation with a lower pressure.

KEYWORDS:

Soft actuator; Silicone; 3D printing; Pneumatic actuators

INTRODUCTION

An actuator is a device that can be categorized as mechanical or electro-mechanical. As its main function, an actuator provides controlled displacements and positions. Traditional actuators can be classified in four categories: electronic actuators, hydraulic cylinders, pneumatic actuators, and motors. Howbeit, traditional actuators have some disadvantages and limitations in size, geometry, and weight.

On the other hand, there is another category of actuators known as flexible or soft actuators. This is a newer technology compared to the everyday actuators mentioned before. Flexible actuators "produce flexible motion due to the integration of microscopic changes at the molecular level into a macroscopic deformation of the actuator material. This can manifest as deflection or volumetric change" [1]. The actuators can be made from a different range of materials like polymers, hydrogels, silicones, and elastomers. The development and research of soft actuators can revolutionize areas like wearable divides, robotics, healthcare, etc. The soft actuators possess some advantages that make them ideal for various applications. They have a low fabrication cost, softness, and freedom for more complex geometries. Inside the soft actuators' categories, it exists the soft pneumatic actuators or SPA which are actuators that actuate by compressed air. Nevertheless, soft pneumatic actuators are not yet fully understood due to the complex properties of the material nature or type of manufacturing [2].

This study will focus into the actuation properties of 3D printed soft pneumatic actuator using silicone, especially in how the properties change when 3D printed with different printing orientations. In the following section, some key principals are explained that are important for understanding soft pneumatic actuators.

CHAPTER I

Literature Review

The chapter addresses key concepts that will be used in the development of the research. For example, the material, hyperelastic models and the FEA simulation.

1.1. Soft pneumatic Technology

1.1.1. Development in Technologies

Soft actuators can be made of different materials that can be synthetic or natural. Depending on the selection of material they are able to transform a stimulus that can be chemical or physical into mechanical work [3]. Over the past years, soft pneumatic actuators have been developed for different types of applications and have been made using different types of manufacturing methods.

In the case of 3D printing, this manufacturing method has not been reviewed in depth unlike other actuators manufactured by a different process [4]. Most of the soft actuators are made of materials like polymers, hydrogels, and elastomers and are manufacture using methods like micro-molding and lithography [5]. The processes mentioned before have some disadvantages. Some of them are requiring manual manufacturing, post processing, assembly, etc. Thus, there is a need of finding new fabrications methods that are less time and resource consuming, which makes 3D printing one of the most viable options that can meet all requirements.

1.1.2. Hyperplastic Materials

Hyperelastic materials like rubbers and silicones have a wide range of applications in a variety of industries, some of them are aerospace, biomedical, etc. The properties that hyperelastic materials possess made them highly attractive. These types of materials have the ability to tolerate large deformations under small loads without losing its original configuration once the load is removed [6]. Moreover, one characteristic of the hyperelastic material is that their stress-strain behavior is non-linear. Because the materials present a small

change in volume, it can be considered as incompressible, meaning that the poisson's ratio is 0.499. [7]

1.1.3. Mooney-Rivlin Model

Before technological development with computers and FEA software, the traditional method for designing with hyperelastic materials was done with hand calculations. The process for calculating the deflections, deformation, etc. was long and most of the times very inaccurate. The engineers had to assume that the material had a linear stress-strain behavior which, in real life, materials show non-linear characteristics [8]. For FEA of hyperelastic models it exists different theories that can be used to simulate the behavior of materials like Neo-Hookean, Ogden, etc. Choosing the best model plays an important role in the results and accuracy of the simulation. In this paper the model that is going to be used is the Mooney-Rivlin model since it is the most stable hyperplastic law [9].

Mooney- Rivlin used the phenomenological theory approach and assumed that the hyperelastic material is incompressible, homogenous and could be model using the Hooke's law [10]. With the considerations mentioned before Mooney came with the following formula that describes the strain energy.

$$W = C_{10}(I_1 - 3) + C_{01}(I_2 - 3) \quad (1) \qquad [11]$$

Where C_{10} and C_{01} are constants and I_1 and I_2 are invariants of the Green's deformation tensor. The invariants of Green's deformation tensor formula are the following:

$$I_1 = \lambda_1^2 + \lambda_2^2 + \lambda_3^2 \quad (2) \qquad [12]$$

$$I_2 = \lambda_1^2\lambda_2^2 + \lambda_2^2\lambda_3^2 + \lambda_3^2\lambda_1^2 \quad (3) \quad [13]$$

Where, λ_1, λ_2 and λ_3 are in terms of principal strain ratios. Formula 1 mentions before is also known as Mooney-Rivlin model and is consider a simple and robust model that can model the behavior of an hyperelastic material. Mooney-Rivlin can be use with 2, 3, 5 and 9 parameters depending on the material.

1.1.4. FEA Procedure

Finite Element Analysis Procedure is a tool that can help simulate and evaluate how a material with a certain geometry under a load is going to behave. The first step for starting a FEA simulation is making the geometry that is going to be used for the testing. Once the geometry is developed, it is important to select a hyperelastic model that can represent the behavior of the material [14]. Since it is a hyperelastic simulation, is important to have the material's mechanical properties. For this, a mechanical testing such as a tensile test can be conducted for obtaining the values in the stress-strain graph. The values need to be added into ANSYS engineering data for obtaining the coefficients of the hyperelastic model selected. Once it is completed, is important to generate a mesh. The element from the mesh needs to have a certain shape for providing acceptable results. ANSYS develop a shape testing for meshing the geometry with the appropriate geometry [15]. Depending on the model and outcomes, the mesh can be modified by making it have more or fewer amounts of elements. After that, the loads can be applied on the faces or geometry of interest.

CHAPTER II

SILICONE AND PRINTER PARAMETERS SELECTIONS

Silicones are inorganic polymers that are highly resistant to low and high temperatures [16] and possess the capability of high elastic deformations. The use of silicone goes from aviation and aerospace to textiles. There are a wide range of silicones with different properties between each other.

2.1. 3D Printing Silicone

Printing silicone materials is a new technology that is being develop. Usually, the way for obtaining soft actuators using a 3D printer is by first printing a cast mold and then pouring the silicone mixture into the cast to obtain the final product. There are also different casting methods like rotomolding, lamination casting, etc. These casting processes are laborious and time-consuming. “Most of the manufacturing steps involved, heavily depend on manual handling that causes fabrication variability and limitations to scientific repeatability” [17]. In mostly all the casting methods “there are restrict possible geometrical shapes, complexity, and scale of the manufactured” [18]. Moreover, obtaining the appropriate viscosity of the silicone for printing can be a challenge, it cannot be too runny that will not permit layering and cannot be too thick that the layers will not be continuous.

Papers published about printing silicone normally use a two-part silicone. The most common silicones mentioned are EcoFlex and Dragon skin. Also, the most frequent thickener agent is Thi-vex. Usually, the printing is done with a printer build by the researchers with two different compartments and a mixing unit attached to the printhead. The mixing unit attached to the printer allows long periods of time printing since the silicone is separated and instantly mixed at the moment of extrusion.

In the case of the UV silicone, there is a method that is being used called drop-off. This technology consists in extruding multiple drops instead of a continuous line and curing it right after. When the curing process is done the next layer can be applied to avoid mixing between layers.

2.2. Specifications for 3D printing

The INKREDIBLE Cellink is a 3D bioprinter. Its main purpose is to be able to print biological material for obtaining tissue, cartilage, and others. Nevertheless, this printer can be considered appropriate for testing and printing silicone due to its characteristics.

The bioprinter has a build volume of 130 x 80 x 50 mm. It has a dual pneumatic extrusion printhead. The dual printhead makes it is possible to work with two different materials or parts of the material at the same time. The printhead works with syringes, thus it only allows the use of liquid materials making it adequate for silicone. Moreover, the bioprinter works with an air compressor that for the initial setup needs to be set at 300 kPa. The flow rate of the material can be easily adapted by increasing or decreasing the pressure in the printer using the knobs located on the right side of the printer wall. The INKREDIBLE has a maximum capacity of 700 kPa but the suggested range is from 5 to 400 kPa. Additionally, the printer has a UV light, having the option of 365 nm and 405 nm. Another advantage of the Cellink it that there are different nozzle diameters that can be attached depending on the requirement of the model and silicone viscosity.

2.3. Materials

For the tests, four different silicones were used. The silicones are EcoFlex 00-30, SORTA-Clear 37, Dragon-skin 10 Fast, and Silicone Solutions SS-5088. The first three silicones are platinum cure silicones that have 2 parts that need to be mixed in a 1:1 ratio for curing and the 4th one is a UV cure silicone. Also, as a thickener agent, Thi-Vex was used in the mixture.

2.3.1. Silicone Preparation

For the testing, different silicones were prepared by different procedures. For the mixture processes of the platinum bases silicones, a stirring rod was used. With the same utensil, the silicones were transferred to a 5 ml syringe. Finally, the silicones were transferred to a special syringe for the INKREDIBLE printer. Below are the processes that were followed according to the type of material.

2.3.2. Dragon-skin 10 Fast

Dragon-skin 10 Fast is a platinum cure liquid silicone with two parts. It is a soft, very stretchy, and super strong silicone (Smooth-on). The silicone cures at room temperature in approximately 75 minutes. After trials, the usable time of the preparation in the INKREDIBLE syringe was determined to be 25 minutes. After that time the silicone becomes very thick compromising the printing results. For the silicone preparation, a thickener agent was used, and the amount was determined by trial and error.

For the first batches, the mixture was prepared using a beaker with 3ml of Part A and a 1ml of Thi-Vex. Moreover, for keeping the 1:1 ratio between part a and b, 3ml of part b was mixed with 1 ml of Thi-Vex in another beaker as well. Right after, both mixes were mingled together, the material was ready to use for the first test. Once the previous method was tried, some modifications were done. For the new procedure, 2 ml of part A and part B were mixed in a beaker and then add 1 ml of Thi-Vex

2.3.3. EcoFlex 00-30

The EcoFlex 00-30 is a platinum-catalyzed silicone with two parts. It has low viscosity, and it cures at room temperature in a lap of 4 hours (Smooth-On). When cured, the silicone is very soft, strong, and very flexible.

The first batch using EcoFlex was a 1:1 mixture of part A and part B as indicated in the instructions.

The second batch was a mixture of EcoFlex and ThiVex. 2 ml of part A with 2 ml of part B were mixed. Then, 2 ml of Thi Vex was added and kept adding until 5ml to get it to the ideal thickness. For the third batch, 2 ml of part A and 2 ml of part B with 1.5 ml of Thi Vex were mingled.

2.3.4. SORTA-Clear 37

SORTA-Clear 37 is a translucent silicone with high viscosity that cures at room temperature in a 4-hour period of time. For the silicone mixture, 2 ml of part A and 2 ml of

part B were mixed. The two parts silicone was thick, for that reason the Thi Vex was not considered necessary. By its own, the mixture was able to layer without a problem.

2.3.5. Silicone Solutions SS-5088

UV silicone is a dual cure. It cures at room temperature in a time gap of 72 hours and after some trials, the curing under UV light was determined to be approximately 4 hours. Since the UV silicone is a one-part silicone and was ready to use from the package, there was no need of mixing it with other solution or part. In the first batch, the silicone was too liquid. For that reason, in the second batch, Thi-Vex was added to see if the thickener will work with the silicone consistency but it did not work.

2.4. Printer Preparation

The following steps were taken to be able to print silicone with the materials previously mentioned.

2.4.1. Printer Calibration and Setup

The following procedure needs to be followed every time the Cellink is going to be use. First, the option “Home axes” needs to be selected. It is important to keep in mind that the syringe and the needle that is going to be used need to be on the 3D printer for getting an accurate calibration. Also, in this step is necessary that the printing bed is clear of any objects and/or materials. By the end, the nozzle should end up in the middle of the printing bed, this will indicate that the home axes calibration was done successfully. If that is not the case, the “Home axes” options should be selected again.

Then, depending on the printing, the z-axis needs to be adjusted. For the testing, the z values used were between 9 and 10 mm. Afterward, using the option “Calibrate Z” the calibration was complete. These steps are crucial for the printing quality and to preserve the good state of the printer. Without the setup, the printer head can be crushed by the bed or if it is set to far away the print object will not have a good result.

On the other hand, the flow rate can be easily adjusted by turning on the head 1 and moving the pressure knob until the ideal flow rate is obtained. For the printing samples of

the UV silicone, the UV light needs to be on. This option needs to be turn on before start printing and turn off once the print is over.

2.4.2. Air Compressor

For running the tests, first, an air compressor was used. The compressor can supply a maximum pressure of 300 kPa. However, when the pressure is higher than 290 kPa the pressure constantly decreased and increased. The compressor was not able to keep a constant pressure at its highest value. For that reason and because some of the tests require higher pressure, the air compressor was changed to a tank that was able reach up to125 psi without losing pressure. The tank was set to 58 psi that is the maximum suggests pressure for the printer by the manufacturer.

CHAPTER III

EXPERIMENTAL SETUP AND TESTING

To recap the concepts discussed in chapter 1, the main goal is to characterize the behavior of a soft actuator using Dragon Skin silicone, chose after results founds in first tests, by simulating the deformations and finding the materials properties. The hyperelastic model that is going to be used in the FEA simulation is the Mooney-Rivlin model and the constants are going to be determine by the program ANSYS with the values manually inserted from the stress-strain graph.

3.1. Validating Ansys Simulation

For the purpose of this thesis, it is important to validate the results obtained from the model developed in ANSYS. The validation is going to be made by comparing the data obtained from the simulations and the experimental data. This process can give us an idea which simulation is more accurate and trustable.

The material used for validation purposes was TangoPlus FLX930. This material possess rubber like qualities. The properties listed in Table 3.1. were obtained from Stratasys Tango Manual and from Wohlers.

	Metric
Tensile Strength	0.8-1.5 MPa
Young's Modulus	27 MPa
Strain	0.0296-0.0555

Table 3.1 Properties of TangoPlus FLX930 [19][20]

The simulation conducted using ANSYS for the tango is an hyperelastic simulation due to the material characteristic. An hyperelastic material can undergo large elastic deformations when subjected to different pressures and has a nonlinear behavior [21]. For that reason, it was necessary to have specific constants to model the materials behavior. ANSYS can provide the information required using the stress-strain curve. The data was

manually inserted using the material properties given in the material's information manual. The stress-strain plot is an approximation using 2 points as seen in Figure 3.1.

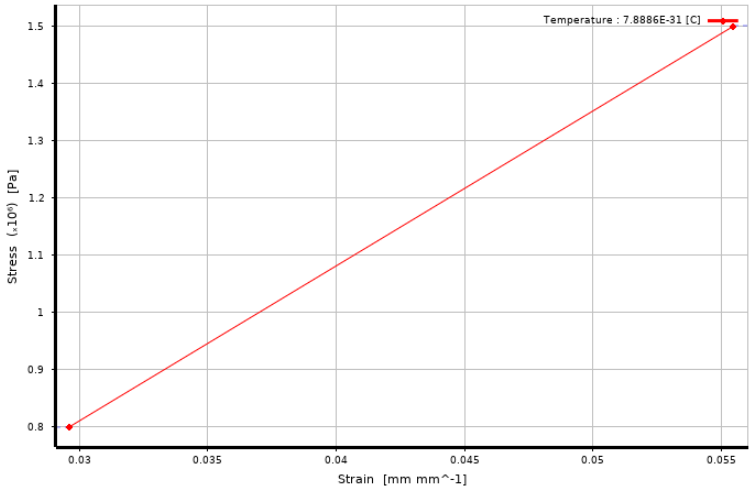

Figure 3.1. Stress vs. Strain plot inserted to ANSYS

The constants obtained from the software using the Mooney-Rivling 2 parameters model where the following.

	Value (Pa)
C_{10}	9.2563E+06
C_{01}	-4.7565E+06
D1	0

Table 3.2. Mooney-Rivling model constants

Furthermore, using the same bellow actuator, 2 models were developed. The first one, Figure 3.2.a, has only one perpendicular pressure acting in all the inner faces of the bellow and the edge of the first bellow chamber is used as a fixed support. In the second one, the pressure is normal to the face for each one of them as seen in Figure 3.2.b to make sure the pressure is better distributed. Also, for this model the edge of the hole is selected as a fixed support.

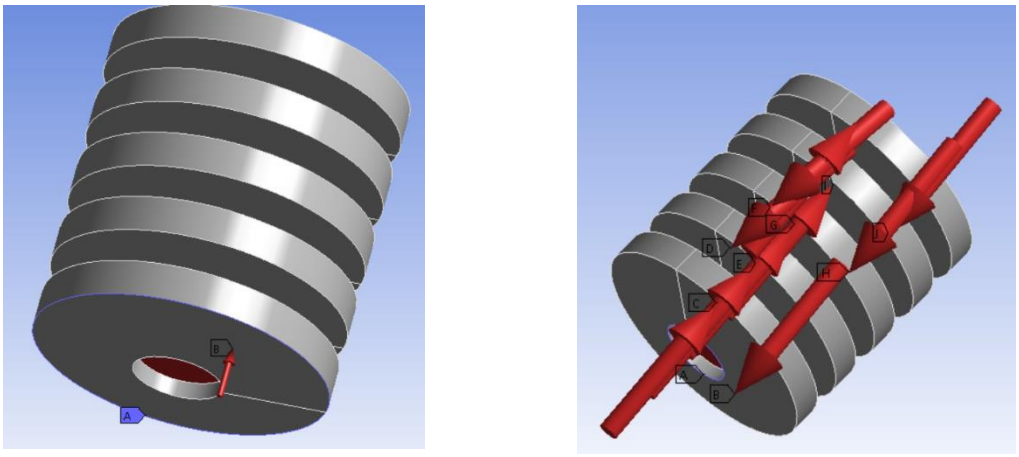

a) *b)*

Figure 3.2. Pressure distribution in the bellow actuator. a) Model 1 b) Model 2

3.2. Actuator Characteristics

The actuator used to conduct the validation of data is a bellow actuator made up with 5 chambers. This type of actuator is expansible and contractible in response to variations in the pressure [22].

The measurements of the bellow are listed in Table 3.3.

Part	Measurements
A	1.23 mm
B	3.24 mm
C	31.46 mm
D	26.53 mm
E	16.26°
F	1.50 mm

Table 3.3 Actuator geometry measurements

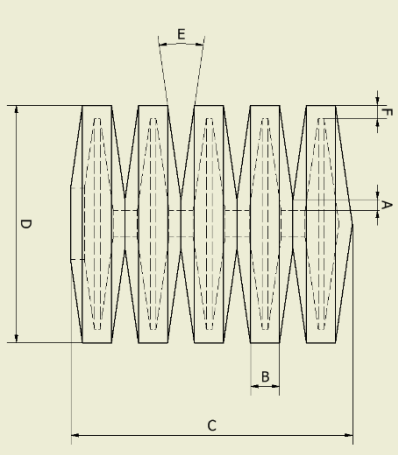

Figure 3.3. Dimensions of bellow

3.3. Test Setup

3.3.1. Fabrication

For conducting a tensile test is necessary to have the sample specimen with the right dimensions. ASTM is an international standard developing organization that set the parameters to follow when testing, the method that is going to be follow is the ASTM D638. The standard is used for determining the tensile properties of plastics using dumbbell-shaped specimens also known as dogbones [23]. Following the standard mentioned, it specifies the specimen dimensions that the dogbones must have to meet for the testing. There are several types depending on the material of interest, in this case the corresponding type, due to the type of material, is Type IV that is for nonrigid plastics. As shown in Figure 3.4, the dimensions are provided with the respective tolerance.

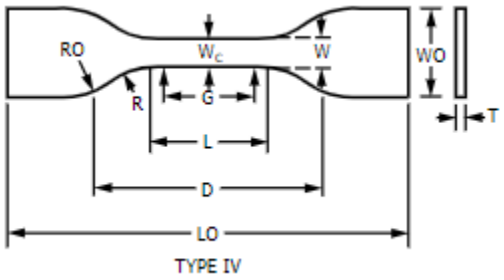

TYPE IV

Dimensions (see drawings)	4 (0.16) or under		Tolerances
	Type IV[B]	Type V[C,D]	
W—Width of narrow section[E,F]	6 (0.25)	3.18 (0.125)	±0.5 (±0.02)[B,C]
L—Length of narrow section	33 (1.30)	9.53 (0.375)	±0.5 (±0.02)[C]
WO—Width overall, min[G]	19 (0.75)	...	+6.4 (+0.25)
WO—Width overall, min[G]	...	9.53 (0.375)	+3.18 (+0.125)
LO—Length overall, min[H]	115 (4.5)	63.5 (2.5)	no max (no max)
G—Gage length[I]	...	7.62 (0.300)	±0.25 (±0.010)[C]
G—Gage length[I]	25 (1.00)	...	±0.13 (±0.005)
D—Distance between grips	65 (2.5)[J]	25.4 (1.0)	±5 (±0.2)
R—Radius of fillet	14 (0.56)	12.7 (0.5)	±1 (±0.04)[C]
RO—Outer radius (Type IV)	25 (1.00)	...	±1 (±0.04)

Figure 3.4. Specimen dimensions used for type IV ASTM D638 [24]

The dogbones were manufacture in two ways. The first one by using a 3D printed mold and the second one by 3D printing directly the specimens. The advantage of 3D printing them directly is that the mechanical properties obtained are more accurate since depending in the printing orientations the properties change and there is absence of bubbles in the specimen.

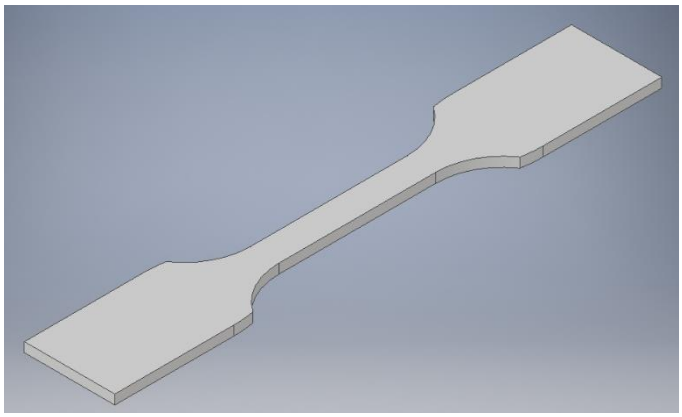

Figure 3.5. Dogbone design in Autodesk Inventor following the ASTM D638 parameters

The mold was design using Autodesk Inventor following the parameters mentioned in the ASTM D3638 as seen in Figure 3.6. For 3D printing the mold the printer used was a MakerBot with an extrusion temperature of 215 ℃. The maximum height permitted is 4 mm, each face of the mold has a depth of 2 mm.

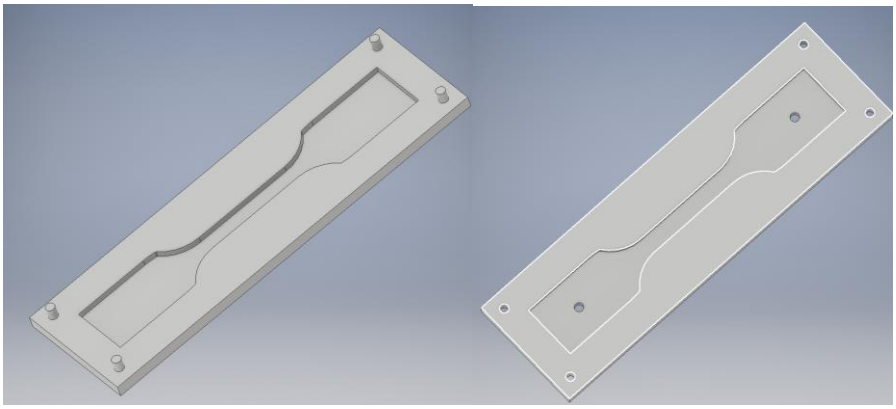

Figure 3.6. Dogbone Mold design in Autodesk Inventor following the ASTM D638 parameters

3.3.2. Tensile Test

The tensile tests were conducted to characterize the mechanical properties of the material and how the printing angle influence in the results. As mentioned above, samples were printed using the Cellink printer. Due to the 3D printing, two sets of samples where printed. The first batch of samples were printed with an orientation of 45° and the second batch of sample with an orientation of 90°.

The tests were conducted following the ASTM D638. The machine used was paired with a load of 50kN. Two tests were conducted, the first test was done with 10 samples, 5 samples of 45° and 5 samples of 90°, to determine the ideal speed for testing since the ASTM D638 suggested 50 mm/min or 500 mm/min as possible speeds. The second test was done with the same number of samples and was to determine mechanical properties since all the samples were tested under the same parameters.

The parameters that were followed for the second testing were: a displacement of 500 mm/min, grips separation of 65 mm.

3.4. Data Processing

After the tensile tests were done, the data collected was process for generating a stress vs strain curve that can model the material behavior based on its properties and the printing direction. Each of the samples tested had between eight hundred and one thousand data. For obtaining a single curve using all the data from each sample an interpolation was done between the strain and stresses. Interpolation was used since the different samples had different amount of data and the time in which the data was taken was not the same. A direct average was not the best method because it would be less accurate and have poor results. MATLAB codes for 45° and 90° are attached in Annex 1 and 2 respectively. For interpolating, first, data from each sample was load and determine the max strain in each. Then, the resolution was selected, in this case it was 0.005 for having a good amount of data and the graph can be more precise. Once that is set, an interpolation is done with respect of the strain. MATLAB is going to start interpolation in 0, then move to 0.005 and see what the stress in that point for each sample is and get the average of those values. Then, the same process is done with 0.010, etc.

3.4.1. Tensile Test Data processing for ANSYS

The obtained curved after the interpolation of the behavior of the material under a uniaxial load described in Method 1 had a zigzag pattern. The load used for the tensile test was 50kPa and the maximum force the dogbone presented was between 1 and 2 N. This huge difference created noise that was reflected in the graph by its pattern. For getting rid of the

noise, a moving average method was applied. The method consists in grouping values and obtaining the average as a new point in the graph. In this case, the group were made by 5 values. After the average, some of the results were still negative and the software Ansys has troubles with negative values in the stress and strain. For that reason, the curve was raised until the lowest point reach 0 to make all the values positives.

3.4.2. ANSYS Setup

First, the data obtained from the curved raised mentioned before was inserted in Engineering data in the uniaxial test data. Once all the data is inserted and because the material is hyperelastic it is necessary to choose one of the hyperelastic models that ANSYS has. In this case Mooney-Rivlin is going to be use. The number of parameters is going to be determined by how good the fit is between the real curved and the generated one.

For the simulations the model 2 was used. The only modification that was done is the fixed support is not the border line but the inner part of it as seen in Figure 3.7.a. and frictionless supports were added on the sides as seen in Figure 3.7.b. The fixed support was changed since it shows a more uniform stress distribution in the bellow and the frictionless support was added for preventing the bellow to bend.

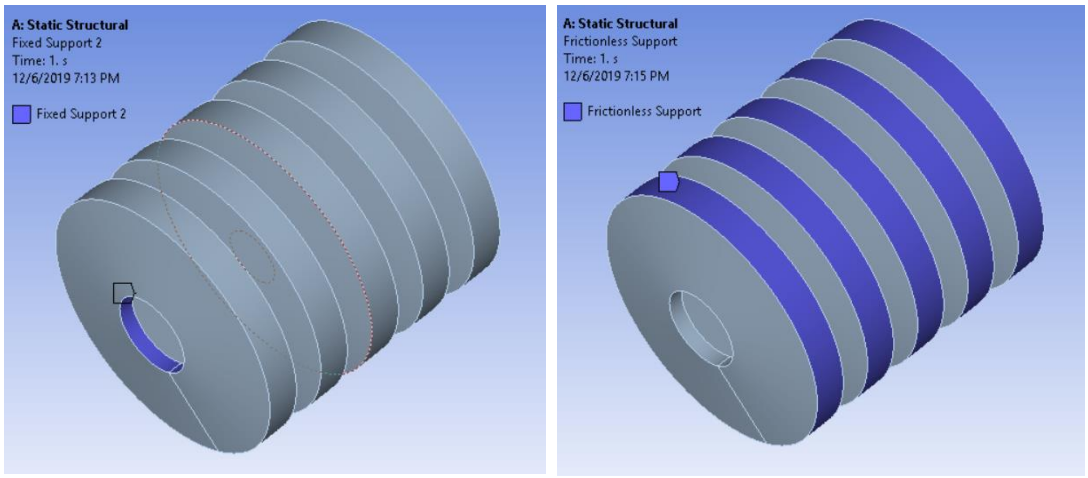

a) b)

Figure 3.7. Supports a) Fixed support b) Frictionless support

For each printing orientation simulations were run. Because there was no physical experiment of a 3D printed bellow actuator the maximum pressure it can resist was unknown. For determining the maximum pressure different simulations were run using an initial mesh of 0.001 m in all the geometry as shown in Figure 3.8.

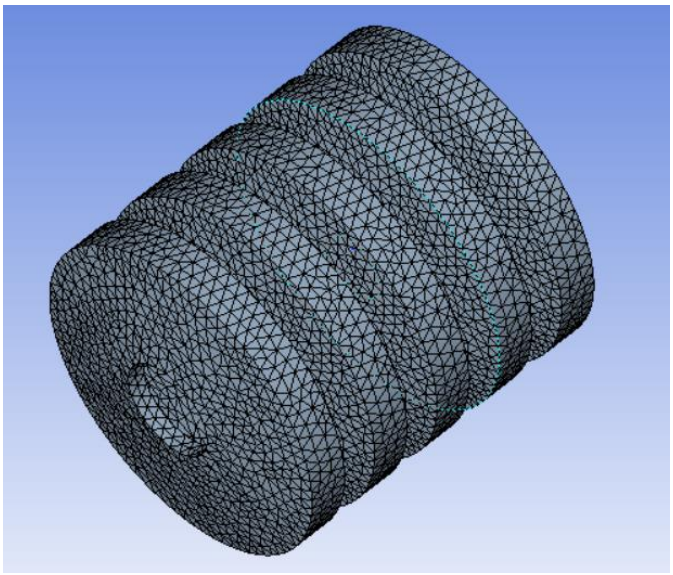

Figure 3.8. Mesh of 0.001 for initial simulations

As is known, the number of elements in a mesh can affect the results. For that reason, a convergence graph is needed. A convergent graph shows how the stress and deformation changes while increasing or reducing the number of elements in a mesh. The graph helps to identify the lowest number of elements needed for obtaining reliable results in the simulation. The smallest size of elements that can be reach is 0.6 mm due limitations in the license of the software. A convergence graph was elaborated for both orientations.

CAPÍTULO IV

RESULTS

3.5. Silicone Results

Silicone	Speed	Pressure	Syringe	Thi Vex	Layering	Cured
Dragon-Skin 10 Fast	4 mm/s	206 Kpa/ 330 Kpa	20G/22G	Yes	Yes	Yes (25 min pot life)
EcoFlex 00-30	7 mm/s	260 Kpa	22 G	Yes	No	No
SORTA-Clear 37	7 mm/s and 4 mm/s	300KPa +	20G	No	Yes	Yes
Silicone Solutions SS-5088	3 mm/s	220 Kpa	25 G	No	No	No

Table 4.1. Results: Different types of silicone

3.5.1. EcoFlex 00-30

All the printing tests were done at a speed of 7 mm/s. The first mixture of EcoFlex as mentioned in section 2.3.3 was too liquid for printing. When the silicone was transferred into the INKREDIBLE syringe, the silicone started flowing out of the needle without any type of pressure. For this test, a 20G needle, which was the biggest one, was used. As a way of solution, the needle was changed into a narrow one of 22 G but the problem was still happening. Since EcoFlex was too liquid, Thi-Vex was added for the second and third batch. From the second batch, a less liquid consistency in the silicone was obtained. The silicone in this batch was able to stay in the syringe without flowing out but was not able to layer because of the low density.

After several hours the mixture did not cure. A possible reason is that the Thi-Vex ratio was too high interrupting the curing process. Regarding the third batch, a less amount of Thi-Vex was added to see the difference in the results. The EcoFlex was still very liquid and had the same problem as the second batch that the mixture did not cure after several hours.

3.5.2. Sorta -Clear

The results from the testing using this material showed that the maximum pressure using the air compressor was not enough for obtaining good printing results. The material was very dense which is good for layering without adding any type of thickening agent. The tests were run starting from 260 kPa until 300 kPa.

For 260 kPa, the pressure was not enough for letting flow in a constant way the silicone making it impossible for it to attach to the surface and start creating good quality layers. For that reason, the pressure was increased until 300 kPa and the printing speed decreased to 4 mm/s. The printing quality was improved but still, the pressure was not enough to keep a constant flow.

3.5.3. Dragon Skin

The firsts tests were run using the first batch method mentioned in 4.1.1 section. The results from these prints were that the silicone was able to flow correctly from the bioprinter and was able to create layers instead of mixing. The problem with this silicone preparation method is that the mix was not able to cure after 24hr. The possible cause is that at the moment of transferring from beaker to beaker part A and B, the ratio was changed.

For that reason, the mixing method was changed as well as the Thi-Vex ratio. The preparation of the second batch is mentioned in the 4.1.1 section. Since this ratio showed good results at the moment of printing, different tests were conducted such as attach to surface, layering, filling, and structure tests.

For the attaching to surface test, a circle with a diameter of 20 mm and a height of 1 mm was used as printing geometry.

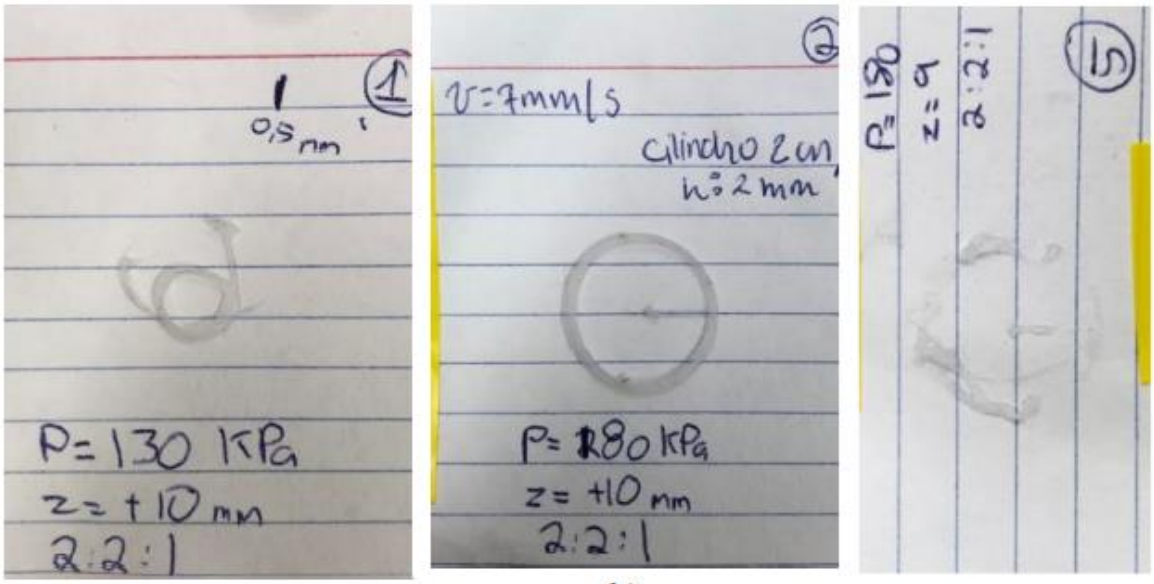

Figure 4.1. Dragon Skin tests using 130 kPa b) Print using 180 kPa c) Print using 180 kPa

The results for the lowest pressure test (Figure 4.1.a) showed that at the pressure of 130 kPa the first layer is not able to attach correctly to the surface due to the lack of flow speed. The first layer issue compromises the quality and result of the subsequent layers. Using a pressure of 180 kPa showed better results. The first layer was able to attach correctly to the base as well as the following layers. The figure 4.1.c showed that after a period of time the Dragon Skin starts to change its properties due to the curing process. It makes it thicker and more difficult to extrude affecting the printing quality. Then, the layering test was run.

For this, the chosen geometry to print was a circle with a diameter of 20 mm and a height of 20 mm.

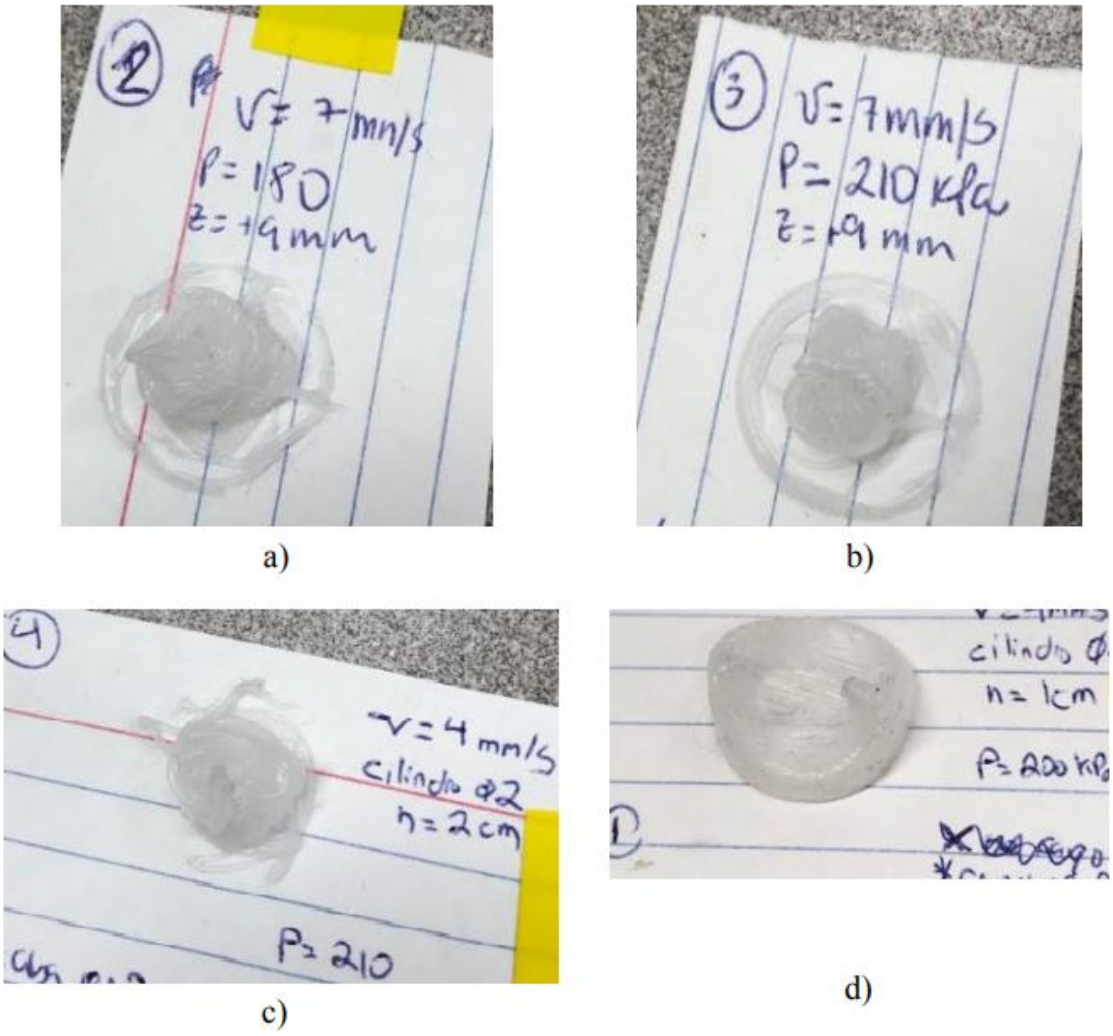

Figure 4.2. Layering test using Dragon Skin a) Test using 180 kPa and 7 mm/s b) Test using 210 kPa and 7mm/s c) Test using 210 kPa and 4 mm/s d) Test using 200 kPa and 4 mm/s

The result of this test showed that the first samples that were printed using a speed of 7 mm/s were not able to layer correctly. Due to the high speed of printing, the layers were not able to attach to the previous one. This has as consequence the formation of a smaller circle in the middle, as shown in figure 5.a and 5.b, affecting the quality of the printing. Using

a speed of 4 mm/s good results were obtained. As shown in figure 5.d, reducing the speed and increasing the pressure made the layers attached correctly one with others. When the print was cured the layers were visible and were attached on to another with no gaps.

Moreover, for the filling test, different geometries were print. The first one is a cylinder with a square hole on top. Then, a circular pyramid and finally a human nose.

The results from the cylinder showed that the perfect printing pressure for the dragon skin using a needle of 20G is 206 kPa. With this pressure, the printing was able to create layers and fill the geometry satisfactorily.

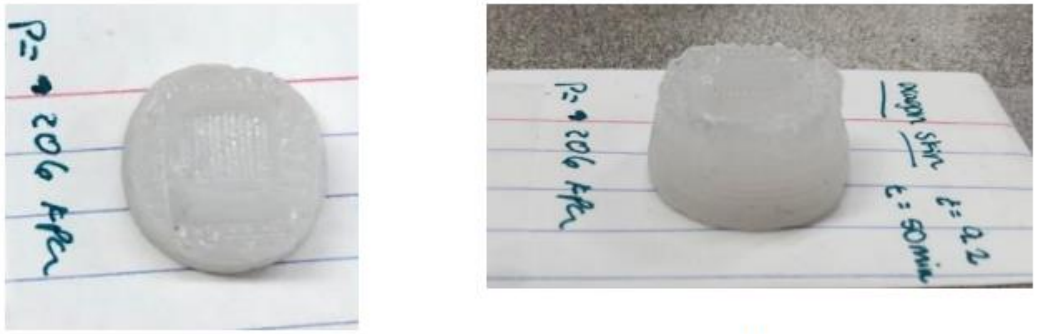

a) b)

Figure 4.3. Cylinder with a printing time of 30 minutes using a printing speed of 4 mm/s a) Top view b) Side view

With this test, the pot life in the syringe for the dragon skin was determined to be 25 minutes.

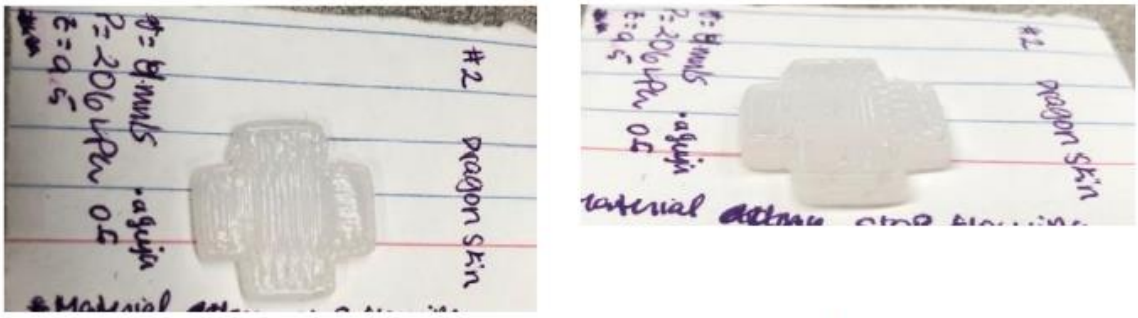

a) b)

Figure 4.4. Cross using a 20G syringe with a printing time of 15 minutes and printing speed of 4 mm/s a) Top view b) Side view

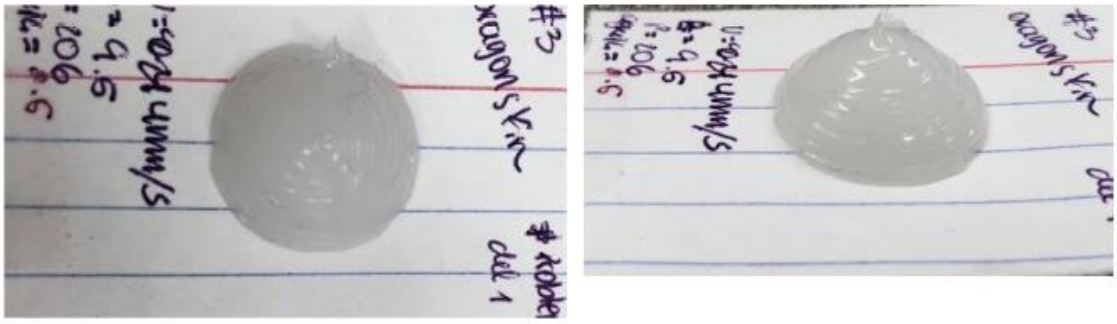

a) b)

Figure 4.5. Circular pyramid using a 20G needle with a printing time of 15 minutes and a printing speed of 4 mm/s a) Top view b) Side view

The samples from figure 4.4 and 4.5 presented the same printing problem. The needle was coming through the printing making it less precise and lowering the printing quality.

The printing results from above had a printing time of 30 minutes. The human nose took approximately 3 hours to print. The first sample was stopped due to the same problem presented in Figure 4.6.

For the second sample of the human nose, the printing was paused every 25 minutes since the preparation of the silicone. This method was used to ensure that during the 3 hours the silicone will flow correctly without getting stuck. During this sample, the problem of the needle coming through the printing. For avoiding the issue, every time a new syringe was changed it was also adjusted to a new height.

Figure 4.6. Human nose printing using a 20G needle with a pressure of 203 kPa at a speed of 4 mm/s.

A possible cause for the needle to cross through the middle of the printing sample is that the bed is not descending enough. The printing layer can be thicker than the descending height of the bed making the needle stuck in the middle of the print. The nose print did not have the best quality of impression. This can probably be due to the needle that was used. Since using a narrower needle means more pressure the air compressor was changed to a tank that let the printer get more pressure.

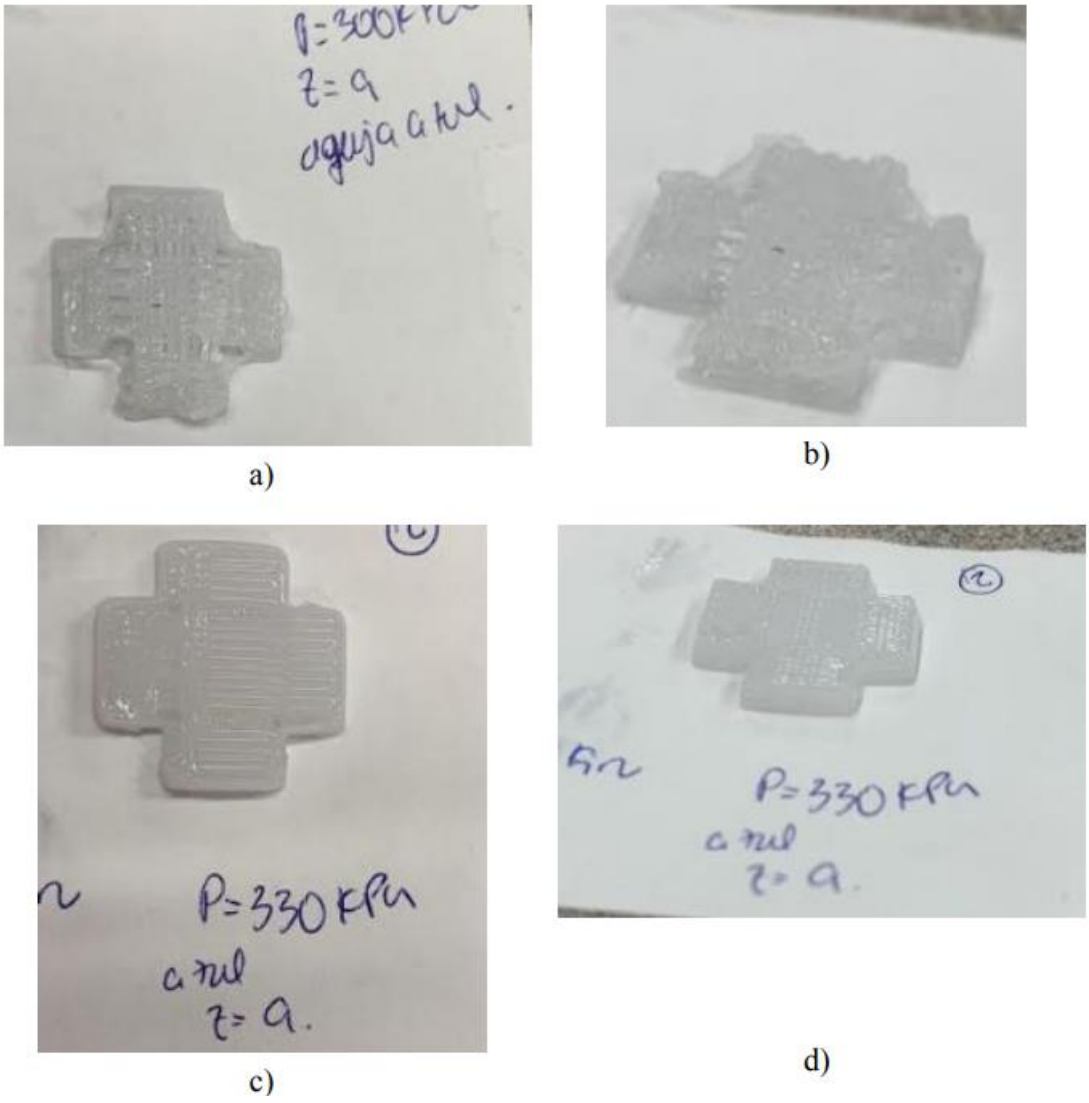

a) b) c) d)

Figure 4.7. Dragon Skin using a 22G needle a) Print with 300 kPa top view b) Print with 300 kPa side view c) Print with 330 kPa top view d) Print with 300 kPa side view

The results showed that the ideal pressure using a 22G needle is 330 kPa. Using this needle, the quality of the impression is better. Furthermore, for these prints, the needle did not come across but for stating this as a solution for that problem taller prints should be tested.

3.5.4. UV Silicone

The first tests were run using a speed of 3 mm/s using a 25 G needle. The silicone, as shown in figure 10.a was too liquid and was not able to create layers. An alternative to this problem was to add Thi-Vex. This procedure was done having not good results. The silicone was very liquid still and probably due to the Thi-Vex the curing properties were affected. Another option was decreased the printing speed to 0.5 mm/s. By doing this, it was pretended to simulate the drop-on process and have more UV light curing time. By leaving a drop of UV silicone under a UV lamp the curing time was estimated to be 4 hours.

3.6. Model Validation

For each model, simulations were run to obtained data using as material Tango. The results were compared with the results obtained using the printed bellow. The values obtained from the experimental test that are going to be compared with the simulation results are shown in Table 4.2.

	Result
Von Misses Stress	3.11 MPa
Displacement	32.4 mm

Table 4.2. Results from the experimental test for comparing with the simulation results [25]

3.6.1. Model 1

The model 1 was run using 15 steps. The maximum pressure that was going to act in the model for finding the stresses was 1.38e+005 Pa and the pressure for comparing the deformation with the values obtained from the printed model was 24.1 kPa. The pressure, in both cases, was increased from 0 to the maximum value in each step gradually.

The results from the simulation were as expected. Using model 1, the total deformation obtained is 0.29 mm which is a very poor deformation amount as seen in Figure 4.8. The model only has a single pressure acting in all the inner faces of the bellow which can be a cause of the results. The pressure distribution using only one direction is not accurate and not well distributed, it does not reflect the real behavior of the printed bellow. The Von

Misses result shows that the maximum stress in the bellow is 0.676 MPa. This result gave us an idea of the points in which the stress is more concentrated.

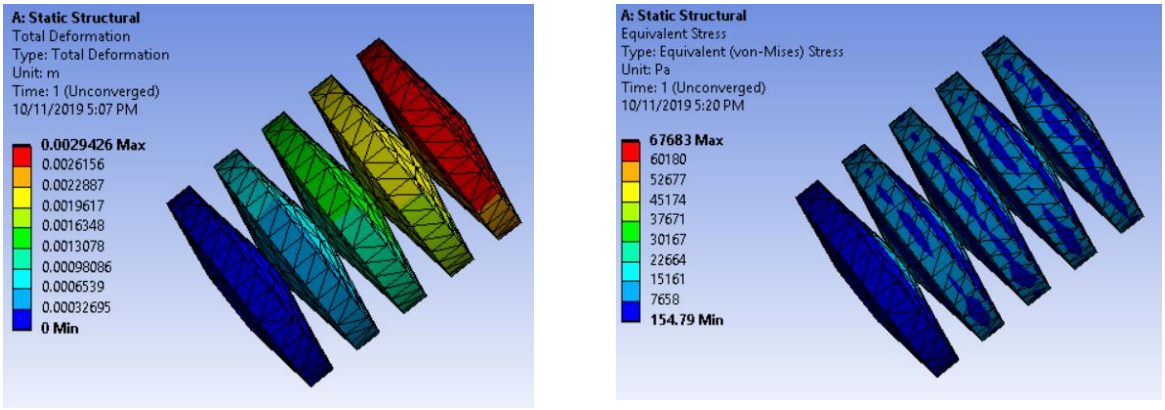

a) b)

Figure 4.8 Results from the simulation of the model 1 actuator. a) Deformation b) Von Mises Stress

3.6.2. Model 2

The Model 2 has multiple pressures located in the inner faces as seen in Figure 3.7.B The pressures have the same values as the Model 1 and are normal to the inner surfaces.

As mentioned before, the maximum pressure that was applied for obtaining the Von Mises stress was 1.38e+005 Pa and for the deformation comparison was 24.1 KPa. The pressure was divided in 15 steps increased gradually for both pressures.

The results from the simulation were better in comparison with the Model 1. The Von Mises stress obtained using the model 2 is 1.97 MPa. In the case of the deformation, the displacement obtained with the second model is 7 mm. The Figure 4.9.a. and 4.9.b. show the results obtained from the simulation.

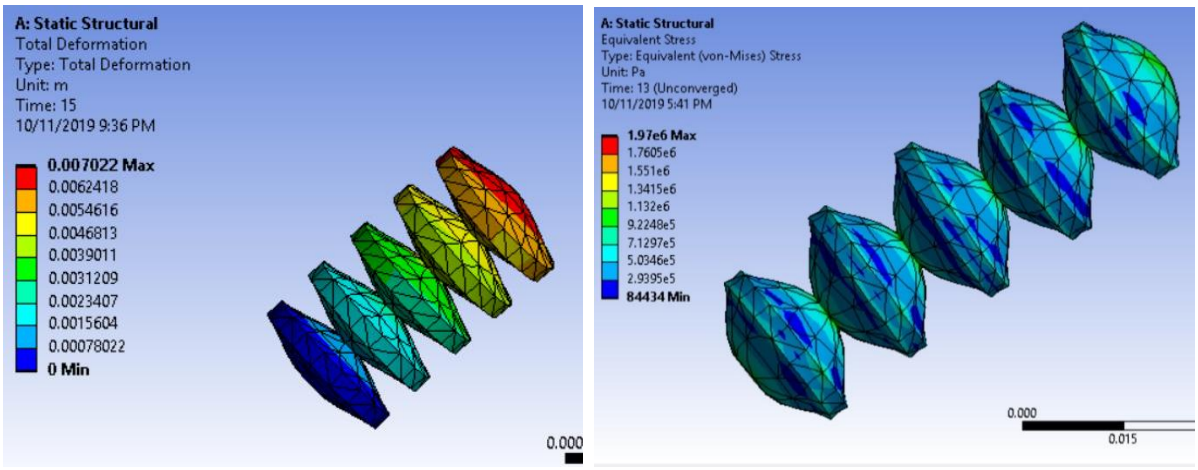

a) b)

Figure 4.9. Results from the simulation of the model 2 actuator. a) Deformation b) Von Mises Stress

The great difference in the elongation can be because, first, the material use for the simulation is 100% TangoPlus FLX930 while the actuator tested in the experimental test is made of a mixture of Formlabs Flexible and Clear Resin. The paper does not give a percentage for each, so it is unknown. Another reason for the difference in elongation can be because of the approximation used in the stress-strain curve for obtaining the hyperelastic constants. Since the information of the stress-strain graph were not available an estimation was done with two points of the stress given in the material properties manual and the Young's modulus. It is known that the Young's modulus is not enough for obtaining a good characterization of the behavior of the material since it is hyperelastic and it can affected on its behavior.

3.7. Tensile Test Results

For the printing angles of 90° and 45° five samples were tested. As mentioned in Chapter I, for processing the data of all the usable samples a code in MATLAB was developed. The main function of the code was to interpolate the stress depending on the strain. The method was used for having data from all samples at the same strain point.

3.7.1. 90° Orientation

The results for 90° showed that only 3 of the 5 tests that were conducted were usable data. 2 of the samples did not reach the breaking point due machine limitations making them not proper data for obtaining the stress strain curve. The other 3 samples had a similar behavior between them and reach a breaking point.

The Graph 2 is the stress vs strain curve for the 3D printed dogbones with an orientation of 90° using a mixture of Dragon Skin 10 Fast silicone and Thi-Vex after the interpolation between the samples. The curve has almost a linear behavior with considerable strain values until the breaking point in 0.063188 MPa.

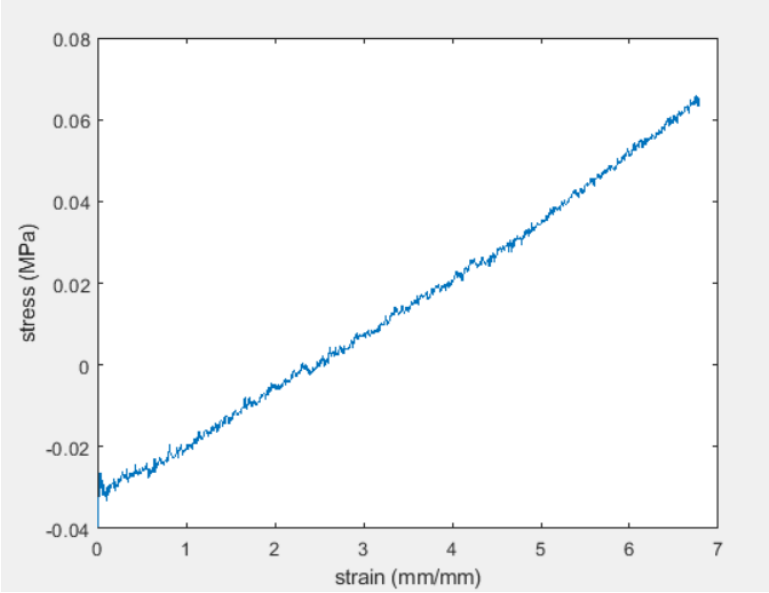

Figure 4.10. Stress vs Srain curve for a 3D printed dogbone

3.7.2. 45° Orientation

On the other hand, the original number of samples printed with a 45° orientation were 5. Due to printing quality one of the samples' results were dismissed in the interpolation for obtaining the graph that describes the behavior of the material. In Graph 3. the stress vs strain

curve for the 3D printed dogbones with an orientation of 45° using a mixture of Dragon Skin 10 Fast silicone and Thi-Vex is shown.

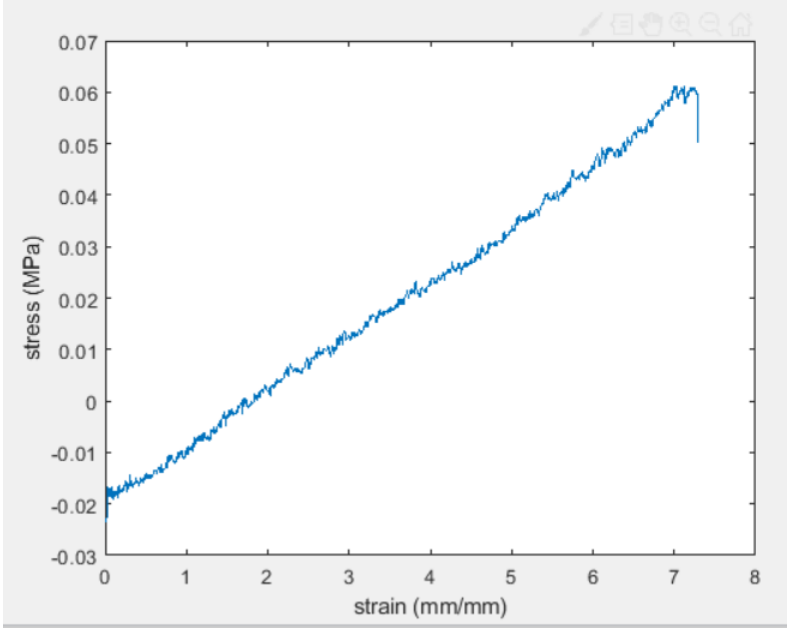

Figure 4.11. Stress vs Srain curve for a 3D printed dogbone 45°

The Stress vs. Strain graph for the 45° dogbones has almost linear behavior with a downfall at the end which is the breaking point at 0.050266 MPa. The maximum strain with the 45° orientation is bigger than with 90°. In Table 4.5 a comparison of the maximum stress and strain in both cases is shown.

Printing angle	Maximum stress (MPa)	Maximum Strain (mm/mm)
45°	0.061241	7.3
90°	0.065703	6.79

Table 4.5. Comparison between maximum stress and strain for 45° and 90°

As seen in the Table 4.5. the results for 90° are higher in stress than the maximum stress for 45°. On the other hand, the samples printed with and orientation of 45° have a higher strain in comparison with the samples printed with an angle of 90°.

3.8. Tensile Test Data Processing for Ansys results

As seen in the Figure 4.10. and 4.11. both 45° and 90°, have considerable amount of noise. The noise makes picks and downfalls across the curves and for reducing the amount of it a running average was done.

3.8.1. 90° Orientation Running Average

After taking averages every five values the Figure 4.12. was obtained as shown below.

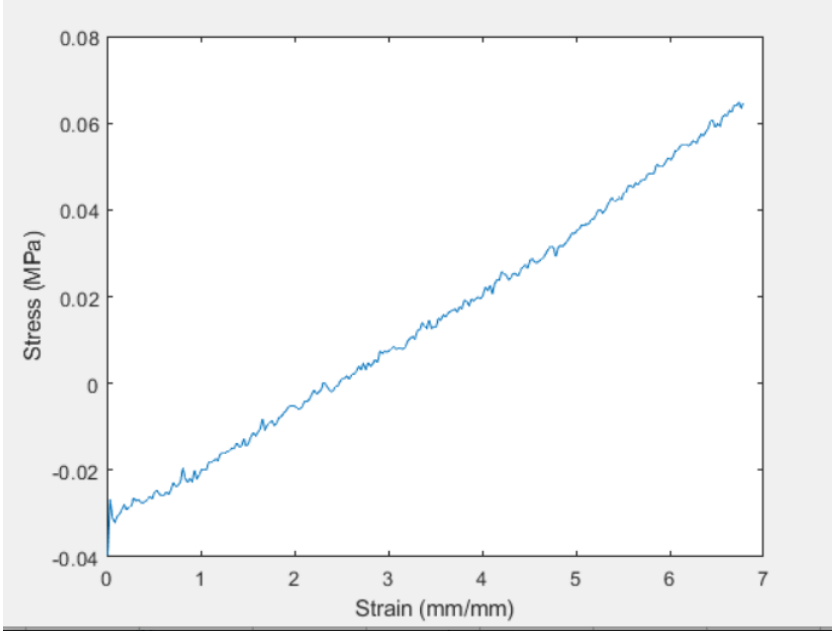

Figure 4.12 New Stress vs Strain curve with the running average for 90°

As seen in Figure 4.12, the amount of noise is less. The curve shape is still the same as the original one but with less picks and downfalls.

3.8.2. 45° Orientation Running average

The same process was done with the data of 45° obtaining Figure 4.13. shown below.

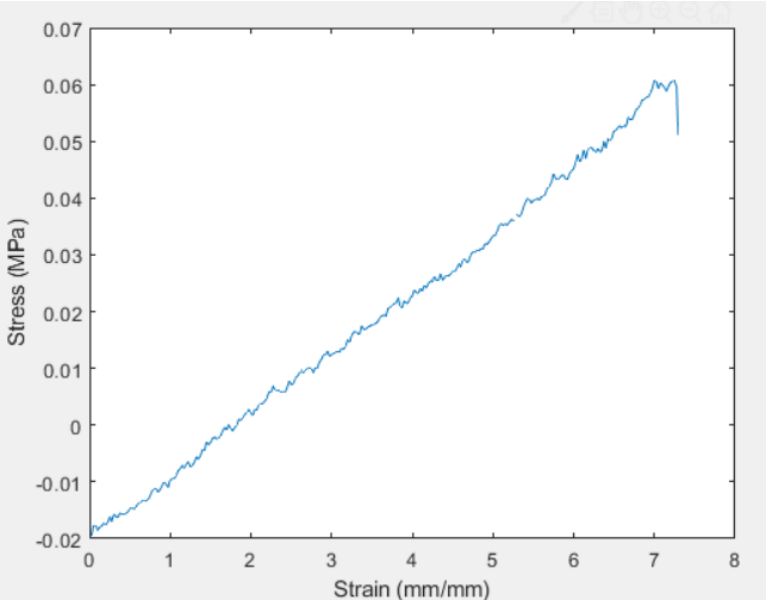

Figure 4.13. New Stress vs Strain curve with the running average for 45°

The graph has the same behavior, the improvement is that the amount of noise is less and there is not as many peaks and downfalls.

3.8.3. Movement of curve to positive

As seen in Figures 4.12 and 4.13, after the running average the curves still with values below zero for the stresses. ANSYS has troubles working with stresses or strains values that are negative, but deleting those values, even though is the fastest option, is not appropriate because it would not be the real material behavior and important data would be delete. Consequently, the lowest point in each graph was moved until it reach 0. The other values were move respectively as well as seen in Figure 4.14.

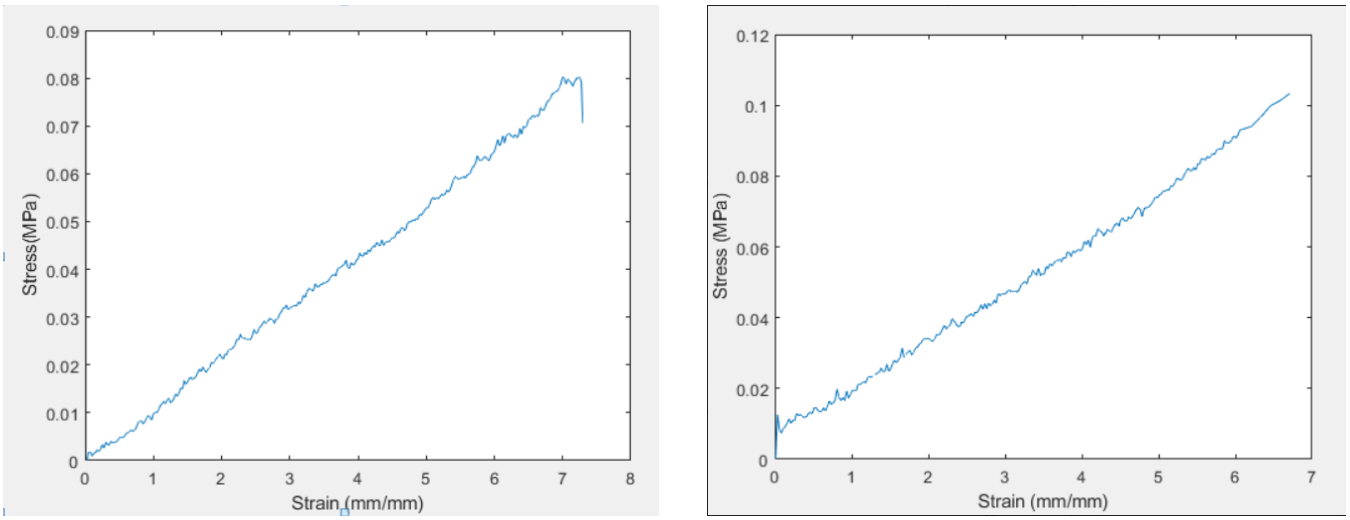

a) *b)*

Figure 4.14. Stress vs Strain curve with new adjustment a) 45° b)90°

3.9. Ansys Simulations

As mentioned in Chapter III, the maximum pressure a 3D printed below can resist was unknown.

3.9.1. 90° Orientation

Before starting with the simulations, it was important to determine the number of parameters that was going to be used. As seen in Figure 4.15, there was three options, 3,5 and 9 parameters.

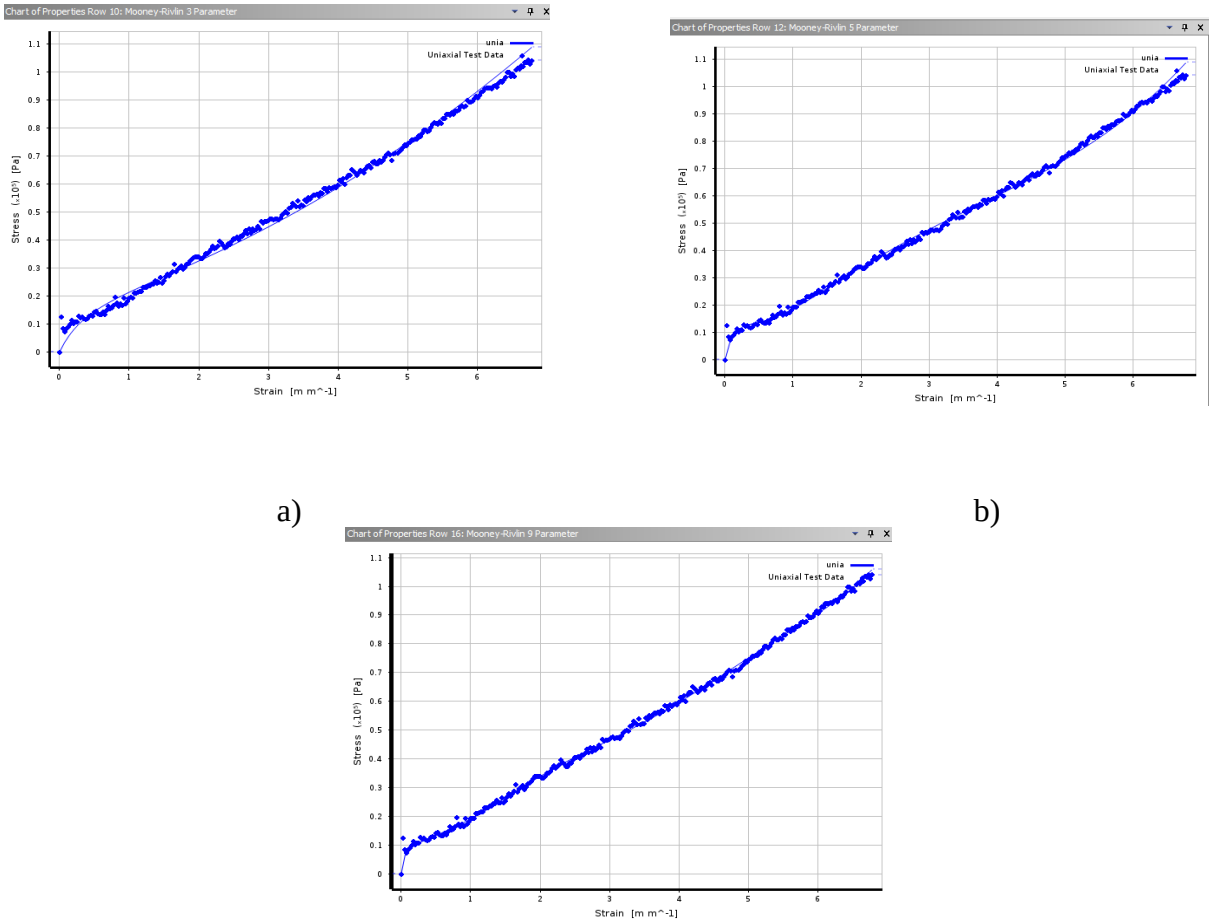

Figure 4.15. Mooney-Rivlin curve fitting a)3 parameters b)5 parameters c)9 parameters

As seen in the Figures above, the fit that Mooney-Rivlin 3 parameters provide is not bad but at the middle of the curve the generated fit is below the points. Also, at the end, the generated fit is far from the original points. In the case of 5 parameters, the fit is better. The generated curve fits good with the original points. At the end of the curve, the generated fit goes up but not as much as in 3 parameters. In the case of 9 parameters, it has a good fit, but the same problems happen at the end as in the other parameters. For the reasons mentioned

before and looking to simplify the model but still get accurate results, Mooney-Rivlin 5 parameter was selected.

Furthermore, multiple iteration with different pressures were done obtaining as a result that for 90° the maximum pressure the bellow can reach is 80 kPa. After running multiple iteration with different pressures there was a characteristic that all the simulations presented. The pattern was that the larger stresses were in the upper and lower part of the bellow chambers. The border did not suffer much stress. Therefore, a bigger mesh can be kept in the borders and apply a thinner mesh in the surfaces that suffer more deformation. The mesh for the sides was kept with 1 mm mesh and the mesh for the upper and lower side of the bellow was changed to obtain the minimum require number of elements. The Figure 4.16. shows how the number of elements affected the stresses.

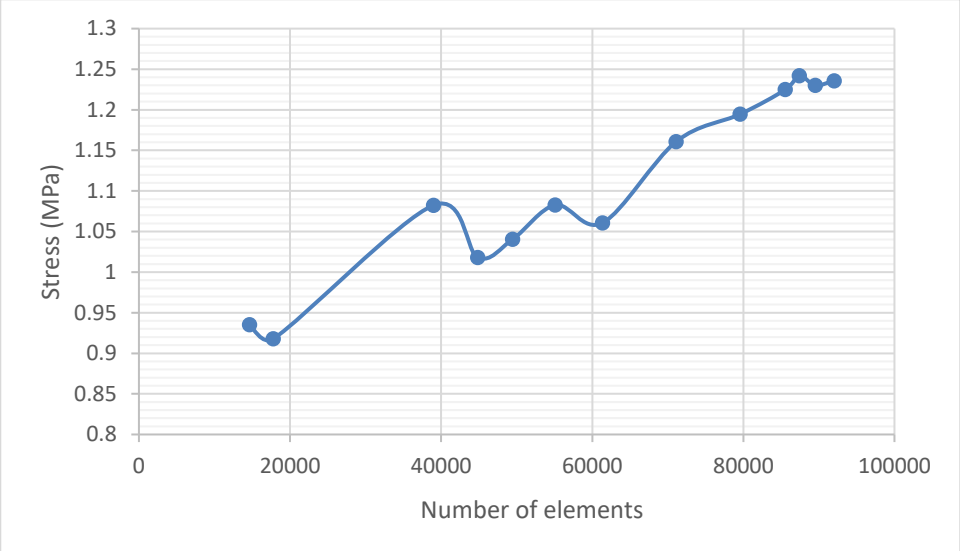

Figure 4.16. Convergence graph, Stress vs. number of elements

As seen in figure 4.16, the mesh with the smaller number of elements presents a lower amount of stress. While the number of elements increases so does the stress until it reaches a point where the variation is null or very small.

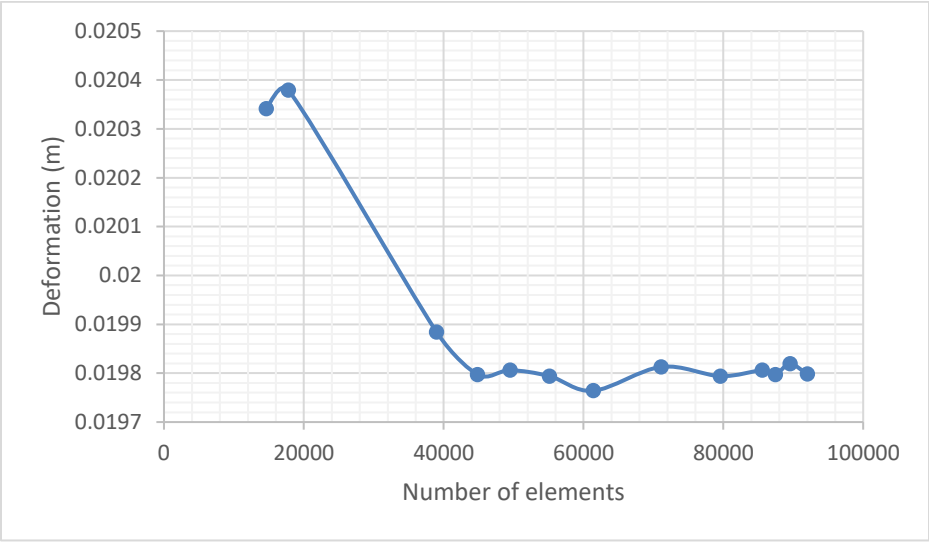

Figure 4.17. Convergence graph, Deformation vs. number of elements

As seen in Figure 4.17 it happens the opposite of Figure 4.16. While the number of elements increase the deformation starts to decrease.

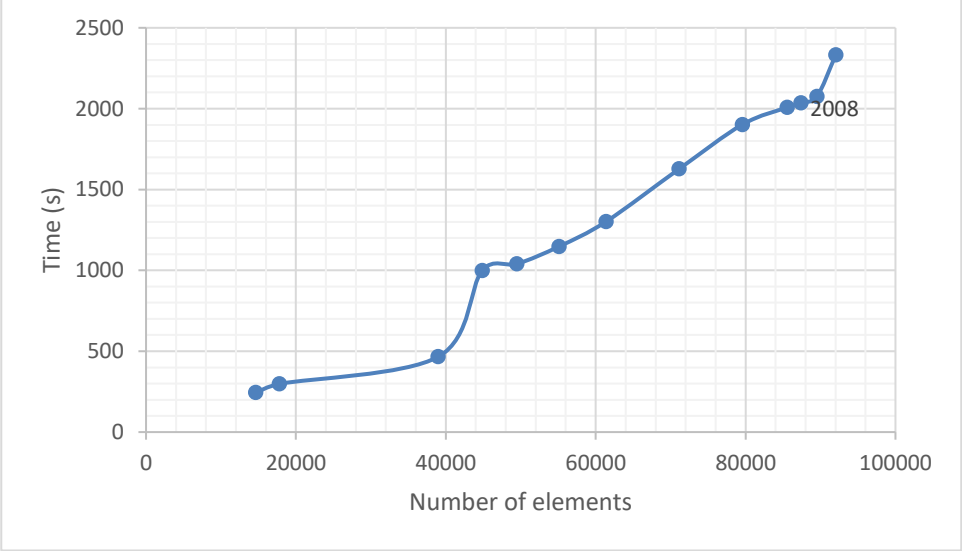

Figure 4.18. Convergence graph, Time vs. number of elements

The Figure 4.18 shows the simulation time depending on the number or elements. The more elements the mesh has the longer is going to take to run the simulation. It is

necessary to find a middle point in which the simulation provides accurate results with a shorter time.

The graphs above provide relevant information for optimizing the simulation. In this case, the difference in the stress is the parameter that is the most relevant for choosing an adequate mesh size. The other parameters as deformation show stable results through different mesh sizes. Figure 4.17 shows that using a mesh with 85570 elements is accurate since the changes in stress are very small and can be negligible.

Using a 0.00063 m elements size (85570 elements) mesh the following results were obtained.

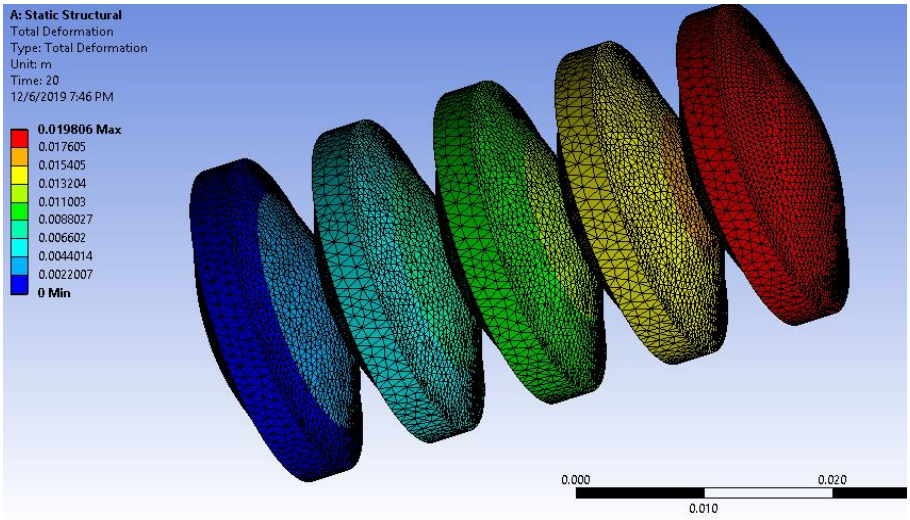

Figure 4.19. Maximum deformation of bellow actuator using a mesh of 0.00063 m in the tops and bottoms of the chamber and a mesh of 0.001 for the sides

The maximum deformation the bellow reaches with a maximum pressure of 80Kpa is 0.0198 m which is equivalent to 1.9 cm. Taking in consideration that the bellow has a length of 3.14 cm the deformation it suffers is almost double its original size.

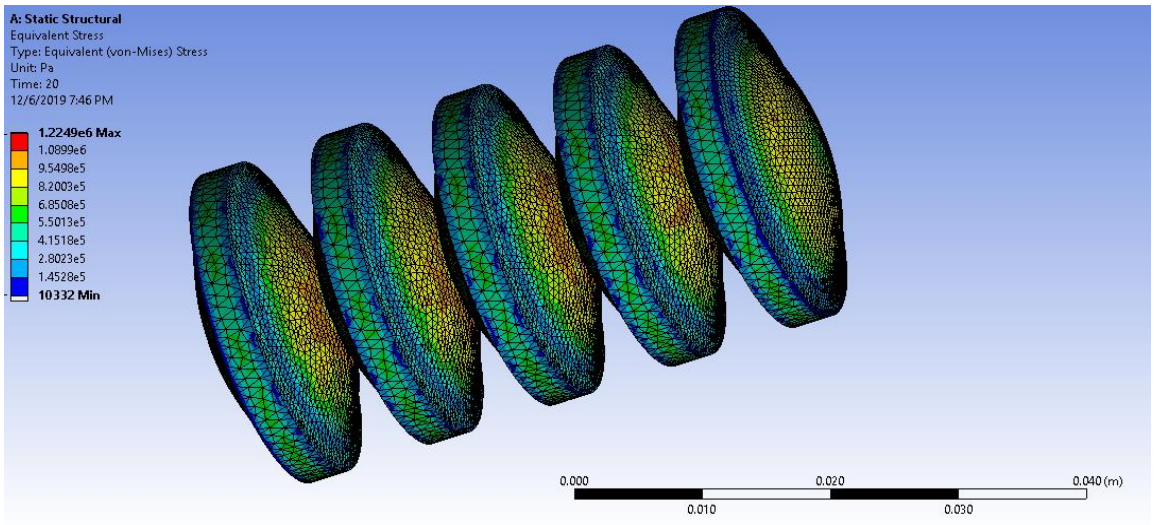

Figure 4.20. Von Mises stress of bellow actuator using a mesh of 0.00063 m in the tops and bottoms of the chamber and a mesh of 0.001 for the sides

The maximum stress the bellow reaches is 1.2249 MPa. As seen in Figure 4.20, the highest stress concentration is in the unions of each chamber and in the inside part of them. This makes sense since it is zone with a big geometry change and is likely to be a stress concentration zone. On the other hand, the sides of the bellow do not have a high stress concentration.

3.9.2. 45° Orientation

As in 90°, before simulation choosing the model parameters is crucial for obtaining good results. Figure 11. shows the different fits depending on the number of parameters.

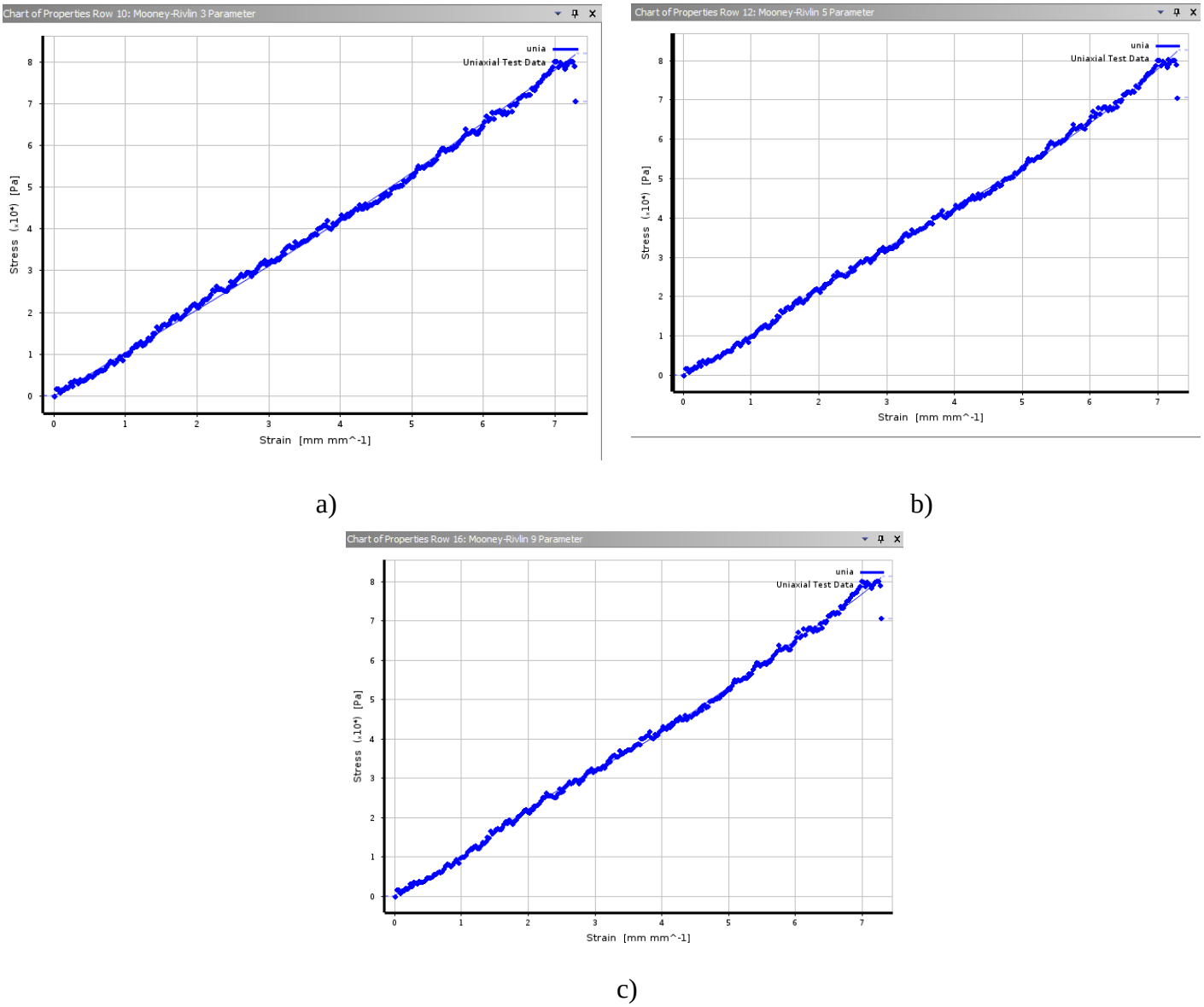

*F*igure 4.21. Mooney-Rivlin curve fitting for 45° a)3 parameters b)5 parameters c)9 parameters

Mooney-Rivlin 3 parameters has a good fit with the original curve but there are some middle parts that are not as close as with the other parameters. In the case of 5 parameters, the curve fits better through all the point of the original curve. The fit of the 9 parameters does not fit well at the las points of the curve. For the reasons mentioned before, the model selected was Money-Rivlin 5 parameters.

Multiple simulations were run with different pressures to determine the maximum value that the bellow actuator 3D printed with a 45° orientation can reach. After multiple iterations, the results showed that the highest pressure that the actuator can reach is 500Pa. As for the simulation for 90°, a convergence graph was developed to choose the less possible number of elements with accurate and reliable results.

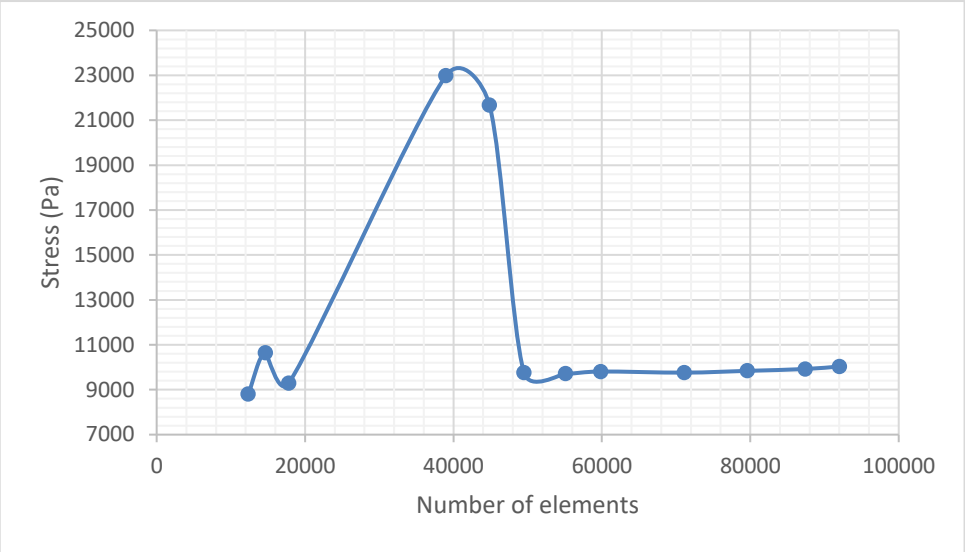

Figure 4.22. Convergence graph for 45°, Stress vs. number of elements

As seen in the Figure 4.22, there is a pick in the stress between 20000 and 50000 elements. After that, the graph stabilizes and does not change considerably even if the number of elements increase.

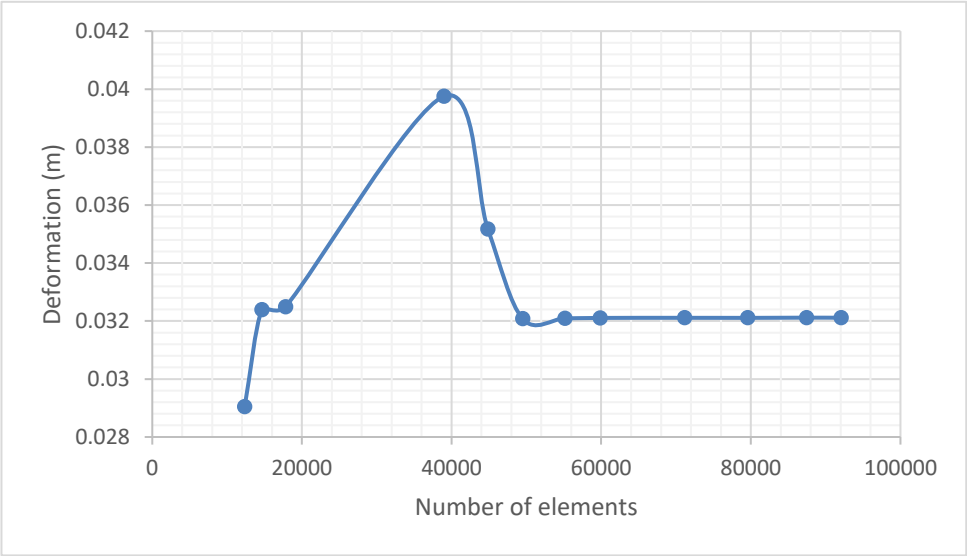

Figure 4.23. Convergence graph for 45°, Deformation vs. number of elements

The highest deformation happens between 20000 and 40000 approximately. After those values, the curve stabilizes in the deformation even if the number of elements increase.

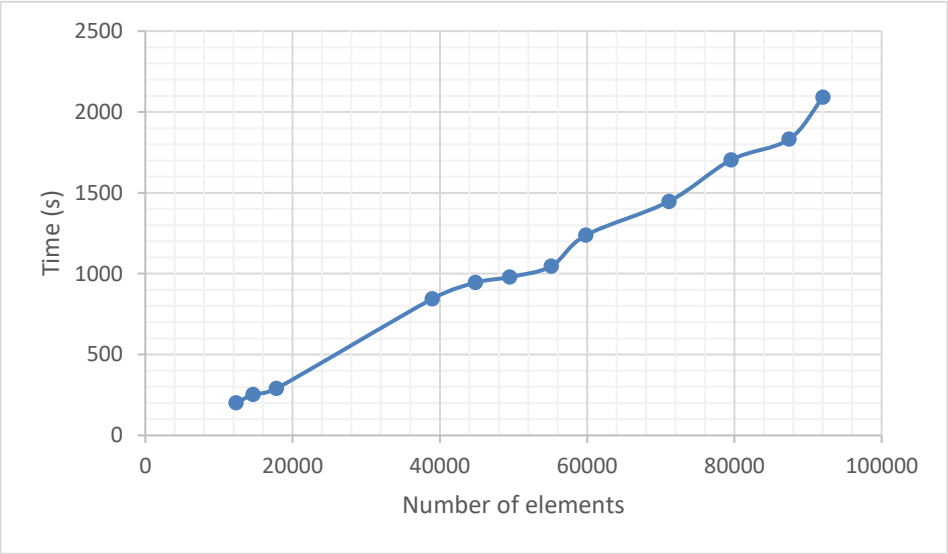

Figure 4.24. Convergence graph for 45°, Time vs. number of elements

The graph time vs number of elements shows the time it takes to run a simulation depending on the number of elements a mesh has. It is directly proportional, meaning that the higher the number of elements, the longer the simulation is going to take.

The graphs above provide relevant information for optimizing the simulation. For 45°, the parameters, stress and deformation, stabilize in a smaller mesh size than in 90°. It means that using a mesh of 49492 elements is enough for obtaining accurate results. The approximate time that is going to take is 979 s that is equivalent to 16 minutes 26 seconds. After the number of elements mentioned, the results are going to have negligible changes and only making the simulation time higher.

Using a 0.00085 m elements size (49492 elements) mesh the following results were obtained.

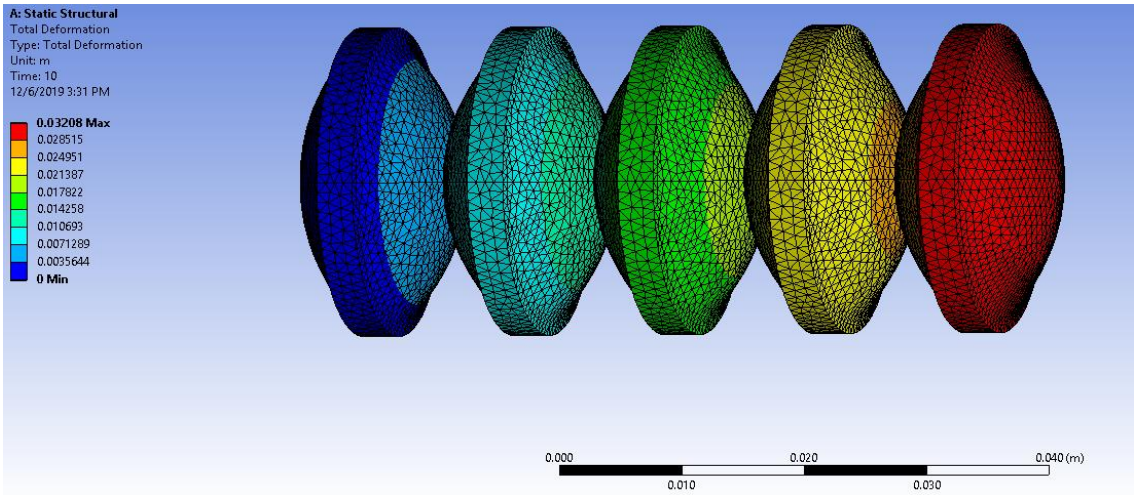

Figure 4.25. Maximum deformation of bellow actuator using a mesh of 0.00085 m in the tops and bottoms of the chamber and a mesh of 0.001 for the sides

The highest deformation obtained with a pressure of 500 Pa is 0.03208 m which is equivalent to 3.2 cm. The bellow suffers a big deformation that is double its size for the small pressure applied.

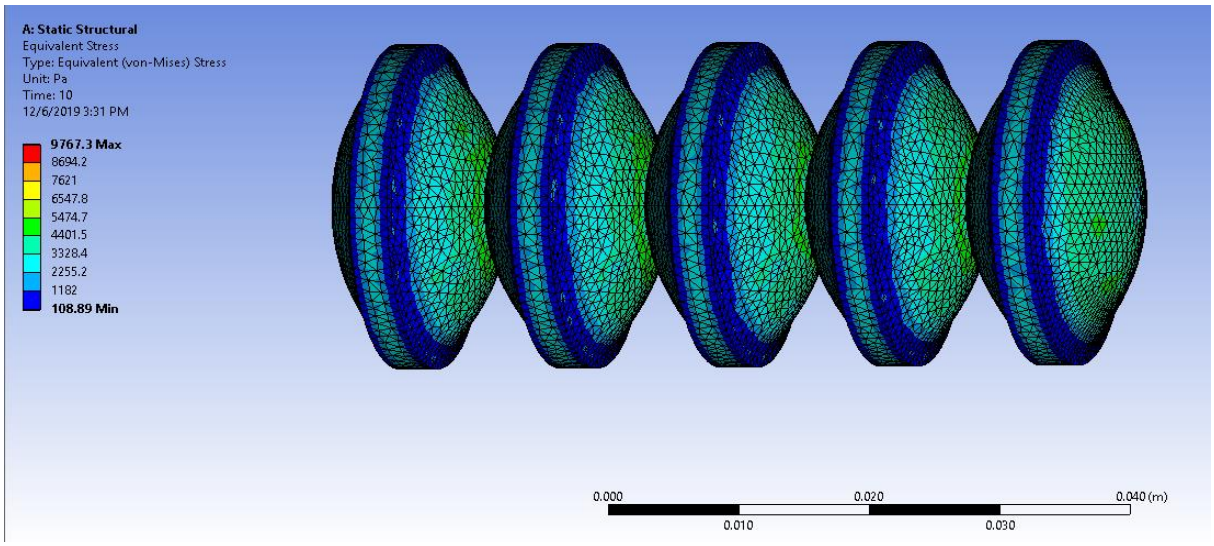

Figure 4.26. Von Mises stress of bellow actuator using a mesh of 0.00085 m in the tops and bottoms of the chamber and a mesh of 0.001 for the sides

As seen in Figure 4.26., the maximum stress is 9767.3 Pa. The areas that suffer the highest stresses are, as in the case of 90°, the outside and inside union of the chamber where is a big geometry change.

CONCLUSIONES

The focus of the paper was to characterize the behavior of a 3D printed bellow actuator and how the manufacturing process and the printing orientation can affect the material mechanical properties.

1. Printing using different silicones and geometries was helpful to evaluate the results. The most common issue with the silicone was that most of them did not have the layering property even though the thickener agent was used. The silicones that were able to create layer were Sorta-clear and dragon skin. With Sorta-clear printing a tall geometry was not possible due to the compressor condition but should be analyzed in the future work.
2. On the other hand, the dragon skin silicone was the one that more testing was able to do due to its properties. The ratio with dragon skin for creating layers was obtained after trial and error. For every 1 ml of each part, A and B, 0.5 ml of Thi-Vex should be applied. The samples from the printing of dragon skin showed that the material and its consistency was able to create layers that attached one to other leaving no gaps in between. Some of the issues presented with the prints were that life of the mix was only 25 minutes which implies being changing the syringes. This could be a problem for prints longer than 2 hours. Another consideration with this method is that the mix of silicone should be done correctly each time to make sure the final product will cure correctly. Also, the needle came across the print causing it to have lower quality and damaging the printing. As a possible solution, a narrower needle was used increasing the printing quality but for the future work, further testing should be done to see if the problem persists. Overall, the silicone that was more printable with good results and properties is dragon skin.
3. After analyzing the numerical results, the bellow printed with 90 degrees orientation was the one that resisted more pressure up to 80 kPa. However, 45 degrees below had larger deformations with less pressure (500 Pa). One reason for the differences in the amount of maximum pressure between the printing orientations can be because 45 degrees printed filaments in the bellow are suffering a cutting force which affects the amount of load that can be resisted. In the case of the 90 degrees printed filaments in the bellow, are orientated in the same direction than the force applied having more resistance to the force applied.

4. Moreover, as seen in the convergence graphs, in the case of 90 degrees printing orientation, stress changes notoriously if the mesh is increased or reduced in the number of elements. In the case of 45 degrees, the number of elements converge in a smaller number and one reason can be due to the fact the pressure is lower. Overall, the convergence graph in the case of 90 degrees started to stabilize at 0.00063 but it would have been interesting to see with smaller elements sizes. This was not able to be done because the ANSYS used had a license with a limited element size.
5. The numerical results from the simulations cannot be proven to be right or wrong, close, or far from the real behavior of the actuator. The bellow actuator had not been tested yet in a real-life experiment so there is not data to compare with. Using a silicone bellow that has been casted cannot give accurate results to compare on how a 3D printed bellow would act since the printings are anisotropic, meaning that depending on the orientation the mechanical properties are going to change. Printing the bellow using the silicone is complicated and still in development. The results give a sense of how the actuator behave but a limitation is that the simulation does not consider the printing orientations and the anisotropy that it has.

REFERENCIAS BIBLIOGRÁFICAS

[1] A. Zolfagharian et al., “Evolution of 3D printed soft actuators,” *Sensors & Actuators: A. Physical*, vol. 250, pp. 258–272, Oct. 2016, doi: 10.1016/j.sna.2016.09.028

[2] Y. Sun, Y. S. Song and J. Paik, "Characterization of silicone rubber based soft pneumatic actuators," 2013 IEEE/RSJ International Conference on Intelligent Robots and Systems, 2013, pp. 4446-4453, doi: 10.1109/IROS.2013.6696995.

[3] K. Asaka and H. Okuzaki, “Soft Actuators: Materials, Modeling, Applications, and Future Perspectives,” *Soft Actuators*, no. 201, p. n., 2014.

[4] A. Zolfagharian et al., “Evolution of 3D printed soft actuators,” *Sensors & Actuators: A. Physical*, vol. 250, pp. 258–272, Oct. 2016, doi: 10.1016/j.sna.2016.09.028

[5] A. Zolfagharian et al., “Evolution of 3D printed soft actuators,” *Sensors & Actuators*: *A. Physical*, vol. 250, pp. 258–272, Oct. 2016, doi: 10.1016/j.sna.2016.09.028

[6] M. Shahza et al., “Mechanical Characterization and FE Modelling of a Hyperelastic Material,” *Material Research*, vol. *18*(5), pp. 918–924, Oct. 2015, doi: 10.1590/1516-1439.320414

[7] P. Barret, “Tips & Tricks for FEA Modeling of Rubber and Elastomers,” *CAEAI*, 2016. [Online]. Available: https://caeai.com/blog/tips-tricks-fea-modeling-rubber-and-elastomers-part-1

[8] O. H. Yeoh, “Hyperelastic Material Models for Finite Element Analysis of Rubber,” *JOURNAL OF NATURAL RUBBER RESEARCH*, vol. 12, no. 1997, pp. 142–153, Oct. 1997.

[9] P. Barret, “Tips & Tricks for FEA Modeling of Rubber and Elastomers,” *CAEAI*, 2016. [Online]. Available: https://caeai.com/blog/tips-tricks-fea-modeling-rubber-and-elastomers-part-1

[10] O. H. Yeoh, “Hyperelastic Material Models for Finite Element Analysis of Rubber,” *JOURNAL OF NATURAL RUBBER RESEARCH*, vol. 12, no. 1997, pp. 142–153, Oct. 1997.

[11] O. H. Yeoh, “Hyperelastic Material Models for Finite Element Analysis of Rubber,” *JOURNAL OF NATURAL RUBBER RESEARCH*, vol. 12, no. 1997, pp. 142–153, Oct. 1997.

[12] O. H. Yeoh, “Hyperelastic Material Models for Finite Element Analysis of Rubber,” *JOURNAL OF NATURAL RUBBER RESEARCH*, vol. 12, no. 1997, pp. 142–153, Oct. 1997.

[13] O. H. Yeoh, “Hyperelastic Material Models for Finite Element Analysis of Rubber,” *JOURNAL OF NATURAL RUBBER RESEARCH*, vol. 12, no. 1997, pp. 142–153, Oct. 1997.

[14] M. Wadham-Gagnon, “Hyperelastic modelling of rubber behaviour in finite element software,” thesis, Library and Archives Canada, Ottawa, 2006.

[15] M. Wadham-Gagnon, “Hyperelastic modelling of rubber behaviour in finite element software,” thesis, Library and Archives Canada, Ottawa, 2006.

[16] ETSU silicone, “What is silicone? : What is silicone made of?,” *Shin-Etsu*. [Online]. Available: https://www.shinetsusilicone-global.com/info/begin1.shtml. [Accessed: 10-Oct-2019].

[17] O. D. Yirmibesoglu et al., "Direct 3D printing of silicone elastomer soft robots and their performance comparison with molded counterparts," *2018 IEEE International Conference on Soft Robotics (RoboSoft*), 2018, pp. 295-302, doi: 10.1109/ROBOSOFT.2018.8404935.

[18] O. D. Yirmibesoglu et al., "Direct 3D printing of silicone elastomer soft robots and their performance comparison with molded counterparts," 2018 IEEE International Conference on Soft Robotics (RoboSoft), 2018, pp. 295-302, doi: 10.1109/ROBOSOFT.2018.8404935.

[19] F. Tango, “Polyjet simulated rubber material,” *Stratasys*, 2018.

[20] J. Mireles, “Appendix E : Material properties Stereolithography,” *Wohlers Report*, pp. 1–59, 2011. [Online] Available: http://www.wohlersassociates.com/materials2011.pdf

[21] SimScale, “Hyperelastic Materials: Simulation Setup,” *SimScale*, 13-Dec-2021. [Online]. Available: https://www.simscale.com/docs/simulation-setup/materials/hyperelastic-materials/. [Accessed: 10-Oct-2019].

[22] G. Immega, “Bellows Actuator,” 26-Jan-1993.

[23] ASTM, “Standard Test Method for Tensile Properties of Plastics,” *ASTM International* , 28-Feb-2017. [Online]. Available: https://compass.astm.org/EDIT/html_annot.cgi?D638%2B14. [Accessed: 05-Oct-2019].

[24] ASTM, “Standard Test Method for Tensile Properties of Plastics,” *ASTM International* , 28-Feb-2017. [Online]. Available: https://compass.astm.org/EDIT/html_annot.cgi?D638%2B14. [Accessed: 05-Oct-2019].

[25] A. Costas, B. Newell, and J, Garcia. “Production and Characterization of a Fully 3D Printed Flexile Bellows Actuator,” *Conference on Smart Materials, Adaptive Structures and Intelligent Systems*, pp. 1–8, Sep. 2019, doi: 10.1115/SMASIS2019-5644

ANEXOS

ANEXO 1: INTERPOLATION CODE 90°

```
file_folder = 'Test_files_90';



Test_1_data = load(strcat(file_folder,'\Test_',num2str(1),'.txt'));
Test_2_data = load(strcat(file_folder,'\Test_',num2str(2),'.txt'));
Test_3_data = load(strcat(file_folder,'\Test_',num2str(3),'.txt'));

Max_strain = min([max(Test_1_data(:,2)), max(Test_2_data(:,2)),
max(Test_3_data(:,2))]);

delta_strain = 0.005;

N_result_file = fix(Max_strain/delta_strain);

final_data_file = [];
for i = 1:1:N_result_file
    value_1 = interp1(Test_1_data(:,2), Test_1_data(:,1),delta_strain*i);
    value_2 = interp1(Test_2_data(:,2), Test_2_data(:,1),delta_strain*i);
    value_3 = interp1(Test_3_data(:,2), Test_3_data(:,1),delta_strain*i);
    final_data_file(i,1) = (value_1 + value_2 + value_3)/3;
    final_data_file(i,2) = delta_strain*i;
end
plot(final_data_file(:,2),final_data_file(:,1))
ylabel('stress')
xlabel('strain')

xlswrite(strcat(file_folder,'/final_results.xlsx'),final_data_file)
```

ANEXO 2: INTERPOLATION CODE 45°

```
file_folder = 'Test_files_45';



Test_1_data = load(strcat(file_folder,'\Test_',num2str(1),'.txt'));
Test_2_data = load(strcat(file_folder,'\Test_',num2str(2),'.txt'));
Test_3_data = load(strcat(file_folder,'\Test_',num2str(3),'.txt'));
Test_4_data = load(strcat(file_folder,'\Test_',num2str(4),'.txt'));

Max_strain = min([max(Test_1_data(:,2)), max(Test_2_data(:,2)),
max(Test_3_data(:,2)), max(Test_4_data(:,2))]);

delta_strain = 0.005;

N_result_file = fix(Max_strain/delta_strain);

final_data_file = [];
for i = 1:1:N_result_file
    value_1 = interp1(Test_1_data(:,2), Test_1_data(:,1),delta_strain*i);
    value_2 = interp1(Test_2_data(:,2), Test_2_data(:,1),delta_strain*i);
    value_3 = interp1(Test_3_data(:,2), Test_3_data(:,1),delta_strain*i);
    value_4 = interp1(Test_4_data(:,2), Test_4_data(:,1),delta_strain*i);
    final_data_file(i,1) = (value_1 + value_2 + value_3)/3;
    final_data_file(i,2) = delta_strain*i;
end
plot(final_data_file(:,2),final_data_file(:,1))
ylabel('stress')
xlabel('strain')

xlswrite(strcat(file_folder,'/final_results.xlsx'),final_data_file)
```